

Deep Learning for Medical Imaging and Clinical Informatics: Preventive and Precision Medicine Perspectives

Le Lu

Ping An Technology US Research Labs (Bethesda, Maryland)
Adjunct Faculty, Johns Hopkins Computer Science & Radiology
Special Volunteer, NIH

lelu@cs.jhu.edu; llu7@jhmi.edu; Le.Lu@pingan.com

Talk slides partially used for Int. Sol Goldman Meeting 2018; GTC Taiwan 2018; CGMH 2018; SNMMI 2018, ISICDM 2018





Q1: Do deep learning and deep neural networks help in medical imaging or medical image analysis problems? (**Yes**)

- ✓ Deep CAD: **Lymph node** application package (52.9% → 85%, 83%) and many CAD Applications
- ✓ Deep Segmentation → Precision Medicine in Radiology & Oncology: **Pancreas** segmentation application package (~53% → 81.14% in Dice Coefficient) and beyond (prostate segmentation, pathological lung segmentation …)
- ✓ Deep Lung (**Interstitial Lung Disease**) Application Package + DL Reading **Chest X-ray**; Pathological Lung Segmentation, ...
- ✓ **Unsupervised category discovery** using looped deep pseudo-task optimization (mapping large-scale radiology database with category meta-labels) → **Learning from PACS!** (CVPR 2015, JMRL 2016, RSNA 2016, WACV 2017)
- ✓ A large-scale **Chest X-ray database** (with NLP based annotation): Dataset and Benchmark (CVPR 2017; CVPR 2018: TieNet: Text-Image Embedding Network for Common Thorax Disease Classification and Reporting in Chest X-rays, MICCAI 2018)
- ✓ **Deep Lesion Graph (oncology cancer imaging)** in the wild: Relationship Learning and Organization of **Significant Radiology Image Findings** in a Diverse Large-scale Lesion Database (CVPR 2018, MICCAI 2018s, RSNA 2018)
- Updates & Publications can be downloaded: www.cs.jhu.edu/~lelu; https://clinicalcenter.nih.gov/drد/staff/le_lu.html;

MICCAI 2018 Young Researcher Publication Impact Award (5 year “test of time” award)!

10/28/2018

Perspectives

Why the previous or current computer-aided diagnosis (CADe; CADx) systems are not particularly successful yet?

- **Integrating machine decisions is not easy for human doctors:** Good doctors hate to use; bad doctors are confused and do not know how to use?
- **Human-Machine collaborative decision making process**

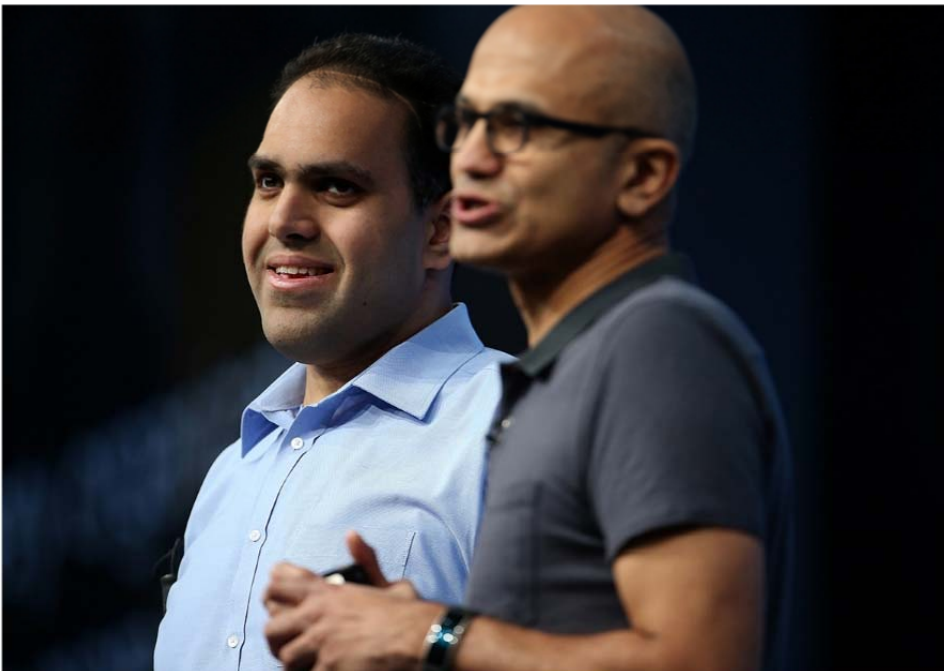
- “Making machine decision more **interpretable, collaborative, explainable**” is very critical for the collaborative system --> learning mid-level attributes or embedding?
- **Preventive medicine:** what human doctors cannot do (in very large scales: millions of general population, at least not economical): → **first-reader population risk profiling** …?
- **Precision Medicine:** a) **new quantitative (segmentation) imaging biomarkers** in precision medicine to **better assist human doctors to make more precise decisions**; b) **patient-level similarity retrieval system** for personalized diagnosis/therapy treatment: show by examples!

Complexity & Composability

The Partnership of the Future

Microsoft's CEO explores how humans and A.I. can work together to solve society's greatest challenges.

By *Satya Nadella*



From left, visually impaired Microsoft developer Saqib Shaikh stands next to CEO Satya



http://www.slate.com/articles/technology/future_tense/2016/06/microsoft_ceo_satya_nadella_humans_and_ai_can_work_together_to_solve_society.html

Three Key Problems (I)

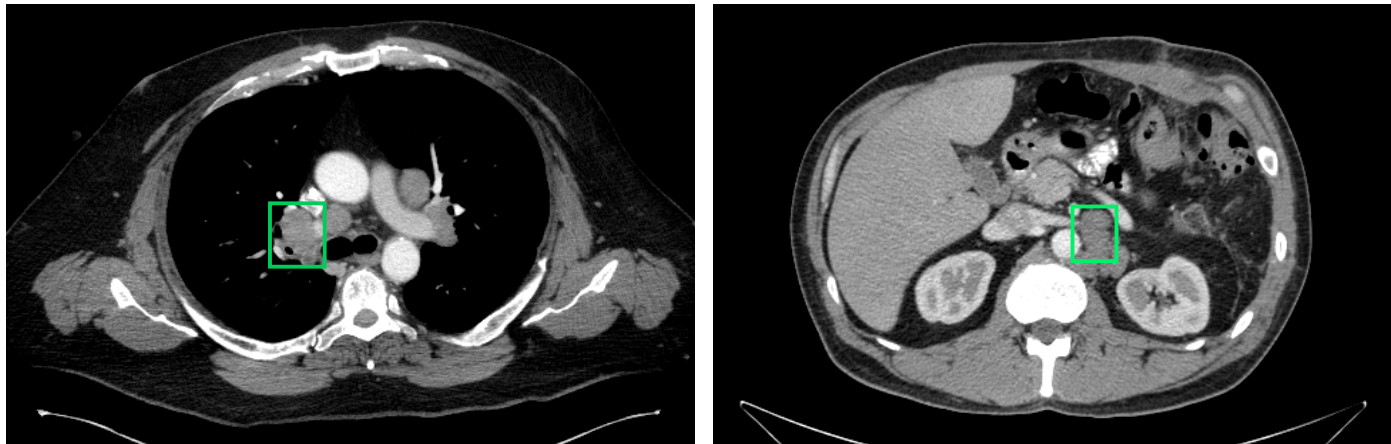
Computer-aided Detection (CADe) and Diagnosis (CADx)

- Lung, Colon pre-cancer detection; Bone and Vessel imaging (6 years of industrial R&D at Siemens Corporation and Healthcare, 10+ product transfer; 13 conference papers in CVPR/ECCV/ICCV/MICCAI/WACV/CIKM, 12 US/EU patents, 27 Inventions)
- **Lymph node**, colon polyp, bone lesion detection using Deep CNN + Random View Aggregation (TMI 2016; MICCAI 2014); **MICCAI Young Researcher Publication Impact Award finalist 2017!**
- Empirical analysis on **Lymph node detection** and **interstitial lung disease** (ILD) classification using CNN (TMI 2016b); prostate CAD (ISBI 2017; MICCAI 2018), Vascular Calcification plaque (ISBI 2017), COLITIS (ISBI 2016), ...
- Non-deep models for CADe using **compositional** representation (MICCAI 2014b) and **+mid-level cues** (MICCAI 2015b); **deep regression** based **multi-label** ILD prediction (*in submission*); missing label issue in ILD (ISBI 2016); ISBI 2017 ...

➤ **Clinical Impacts:** producing various ***high performance*** “second or first reader” **CAD use cases** and applications → effective imaging based prescreening (triage) tools on a cloud based platform for large population preventive profiling

Automated Lymph Node Detection

- Difficult due to large variations in appearance, location and pose.
- Plus low contrast against surrounding tissues.

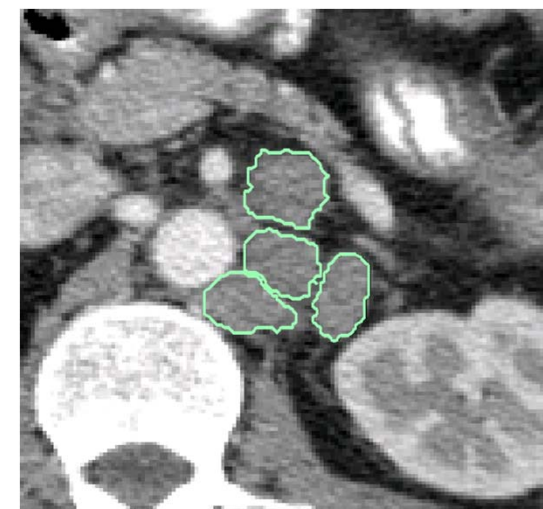


Make Shallow to Go Deeper via Mid-level Cues?

[Seff et al., MICCAI 2015]

- We explore a learned transformation scheme for producing enhanced semantic input for HOG, based on LN-selective visual responses.
- Mid-level semantic boundary cues learned from segmentation.
- All LNs in both target regions are manually segmented by radiologists.

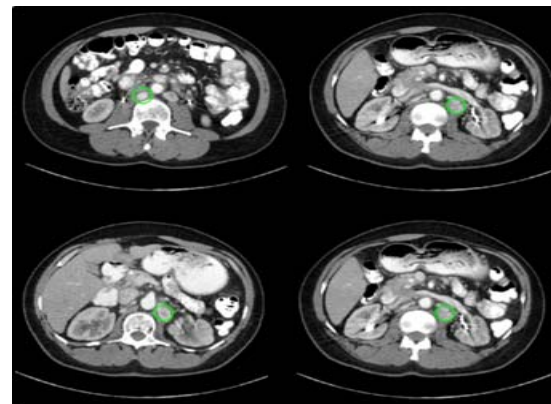
Target region	# Patients	# LNs
Mediastinal	90	389
Abdominal	86	595



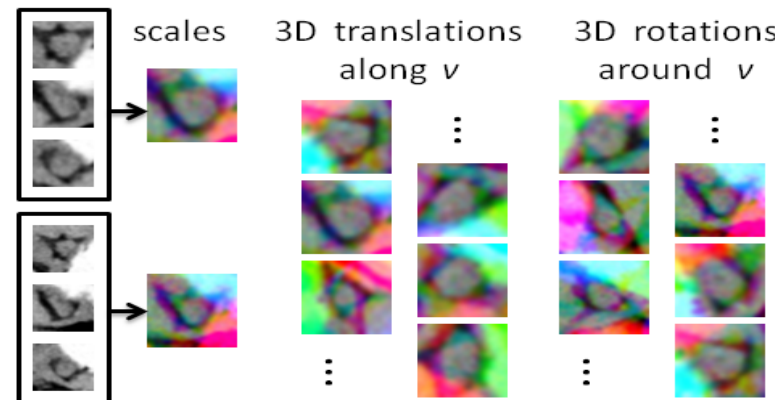
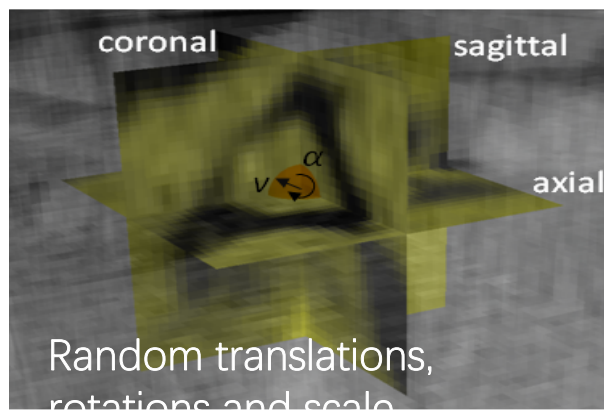
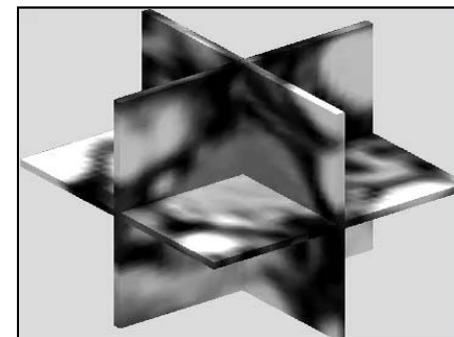
NDSEG Fellow,
CS PhD student,
3rd year, Princeton

Deep models: Random Sets of Convolutional Neural Network Predictions via Compositional Representation

[Roth et al. MICCAI 2014, Shin et al. TMI 2016; Roth et al. TMI 2016]

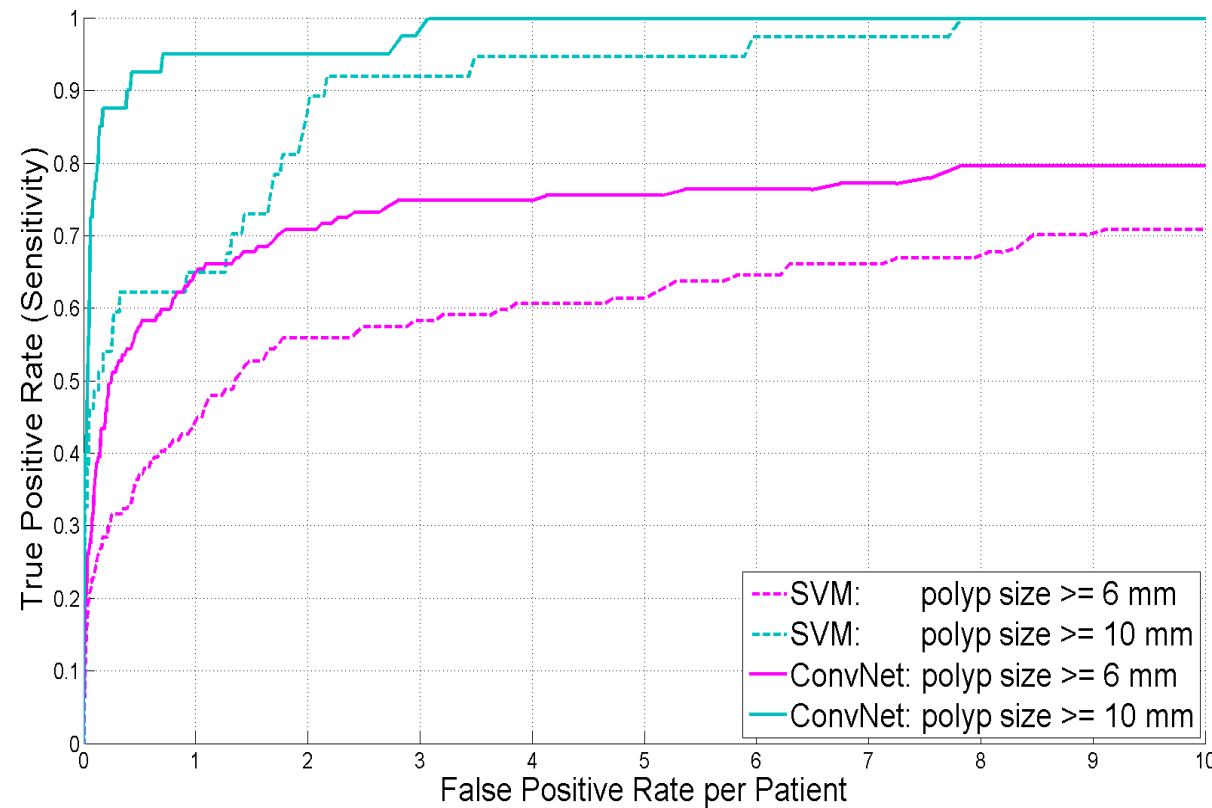


Application to appearance modeling and detecting lymph node

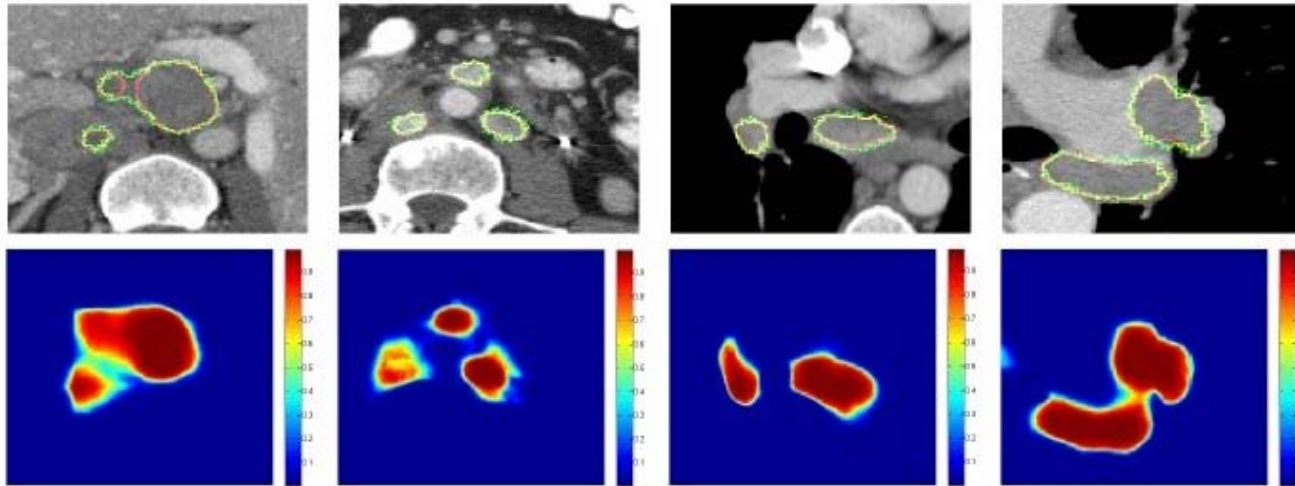


Senior Research Scientist, NVIDIA

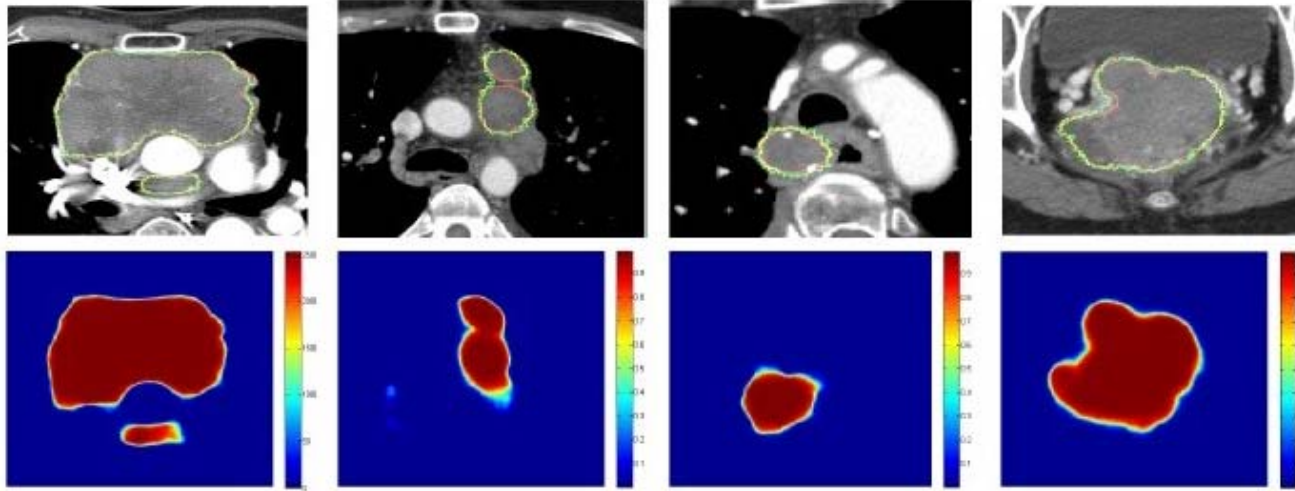
Generalizable? Colon CADe Results using a deeper CNN on 1186 patients (or 2372 CTC volumes) via fine-tuning AlexNet [Roth et al., TMI 2016]



[**SVM** baseline] Summers, et a., Computed tomographic virtual colonoscopy computer-aided polyp detection in a screening population, Gastroenterology, vol. 129, no. 6, pp.1832–1844, 2005



2nd year PhD
student, NSF
Fellow, Harvard



[Nogues et al., MICCAI 2016]

MICCAI 2016 Travel Award

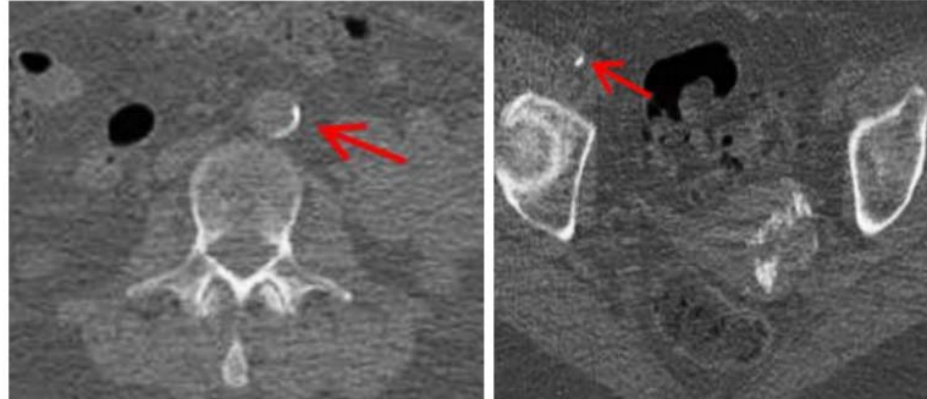
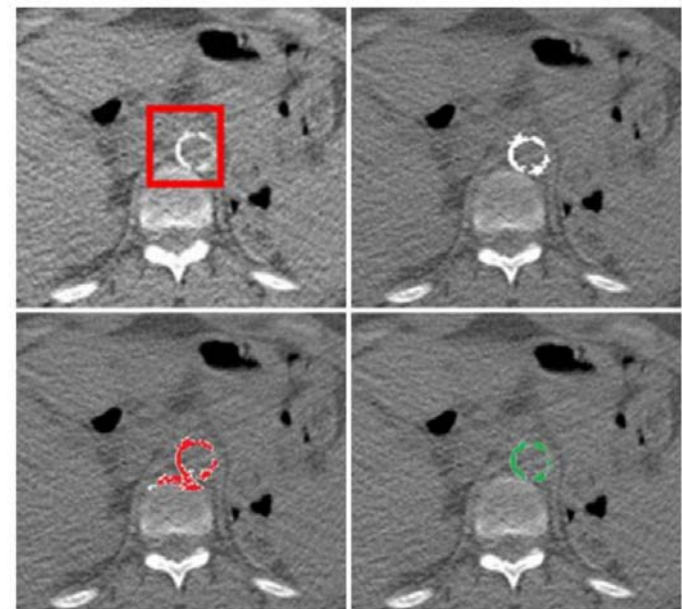
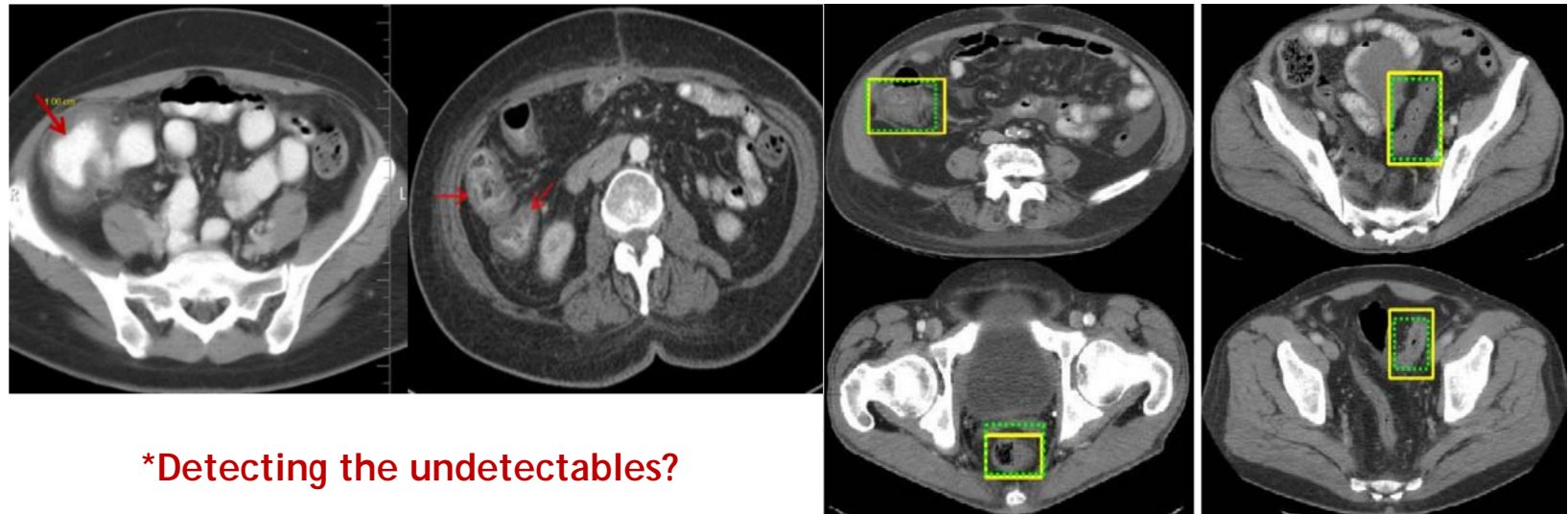


Figure 1. Examples of calcified plaques (red arrows) on abdominal (left) and pelvic (right) CT scans.



Atherosclerotic Vascular Calcification Detection and Segmentation on Low Dose Computed Tomography Scans ···, Liu et al., IEEE ISBI 2017



*Detecting the undetectables?

*Fitting in practical/real clinical
settings in the wild??

COLITIS DETECTION ON COMPUTED TOMOGRAPHY USING REGIONAL CONVOLUTIONAL NEURAL NETWORKS, Liu et al., IEEE ISBI 2016

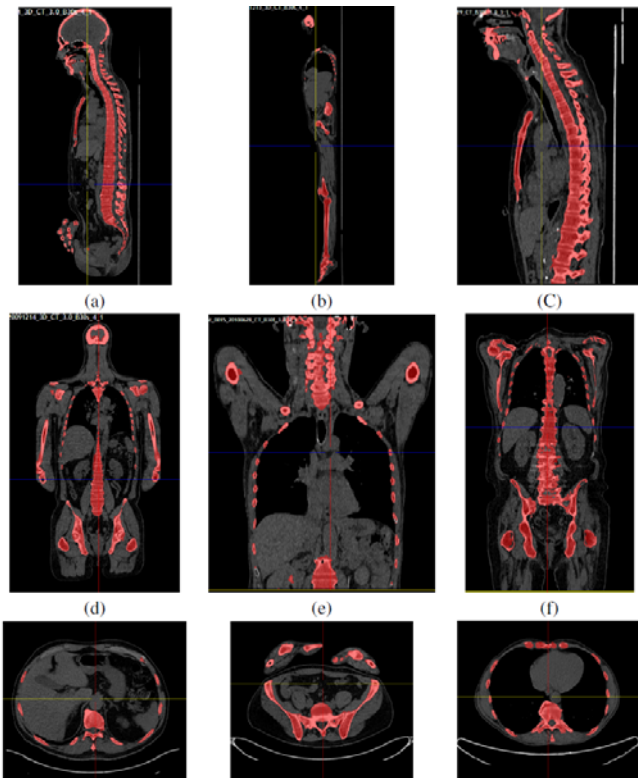
Three Key Problems (II)

Semantic Segmentation in Medical Image Analysis

- “DeepOrgan” for **pancreas segmentation** (MICCAI 2015) via scanning superpixels using multi-scale deep features (“Zoom-out”) and probability map embedding.
- Deep segmentation on **pancreas** and **lymph node clusters** with Holistically-nested neural networks as building blocks to learn unary (segmentation **mask**) and pairwise (labeling segmentation **boundary**) CRF terms + spatial aggregation or + structured optimization, ISBI 2016, MICCAI 2016.
- The focus of recent MICCAI 2016-2018 papers since this is a much needed task → **Small datasets; (de-)compositional** representation is still the key. **Scale up** to thousands, thousands of patients if not more than that; **weakly supervised** segmentation → **Effective and Efficient Precision Biomarkers, even predicting the Prognosis Tumor Growth** (DL tumor growth model prediction MICCAI 2017, TMI 2018, MICCAI 2018)

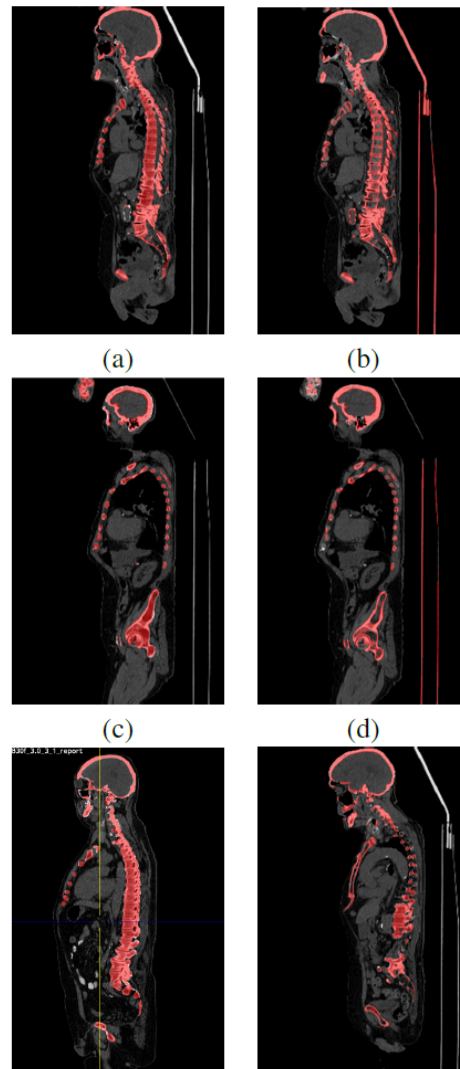
➤ **Clinical Impacts:** semantic segmentation can help compute clinically more accurate and desirable precision imaging bio-markers or measurements → precision imaging personalized treatment and therapy → **Less Guess More Doing** (beyond RECIST 1.1)…

Semantic Segmentation on PET-CT Patient Imaging (pathological ...)



*robust, precision/accuracy, speed!

10/28/2018



Towards whole Body precision measurements or computable precision imaging biomarkers



"Robust Whole Body 3D Bone Masking via Bottom-up Appearance Modeling and Context Reasoning in Low-Dose CT Imaging", Lu et al., IEEE WACV 2016



Bone Mineral Density (BMD) scores, Muscle/Fat volumetric measurements in whole body or arbitrary FOV imaging ... lung nodules, bone lesions, head-and-neck radiation sensitive organs, segmenting flexible soft anatomical structures for precision medicine, all clinically needed!

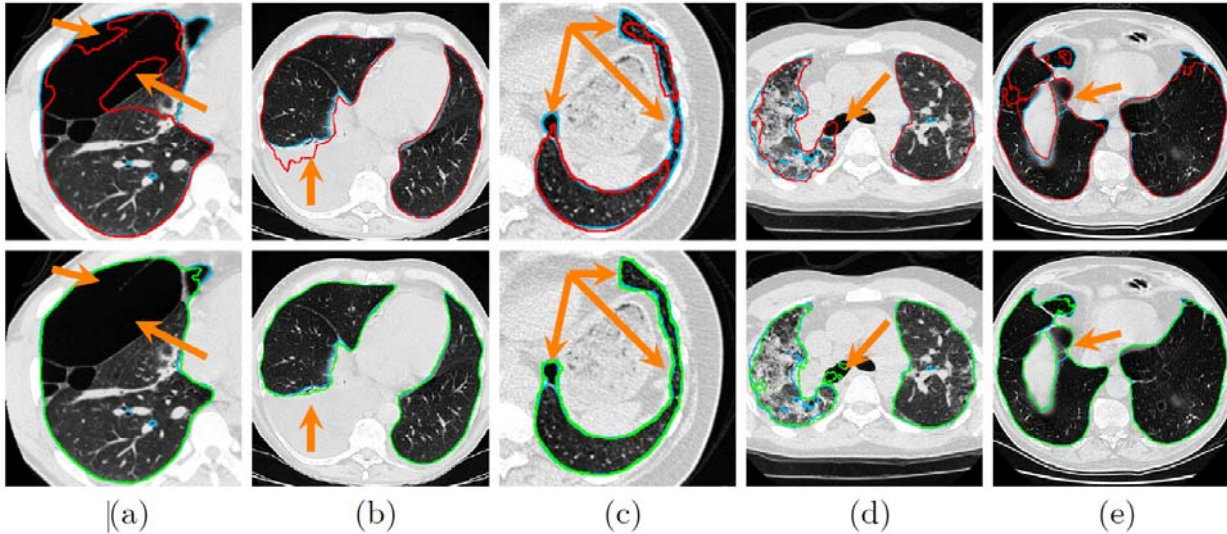


Fig. 2: Example masks of HNN and P-HNN, depicted in red and green, respectively. Ground truth masks are rendered in cyan. (a) HNN struggles to segment the pulmonary bullae, whereas P-HNN captures it. (b) Part of the pleural effusion is erroneously included by HNN, while left out of the P-HNN lung mask. (c) P-HNN is better able to capture finer details in the lung mask. (d) In this failure case, both HNN and P-HNN erroneously include the right main bronchus; however, P-HNN better captures infiltrate regions. (e) This erroneous ground-truth example, which was filtered out, fails to include a portion of the right lung. Both HNN and P-HNN capture the region, but P-HNN does a much better job of segmenting the rest of the lung.

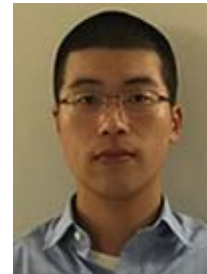


NSERC Fellow

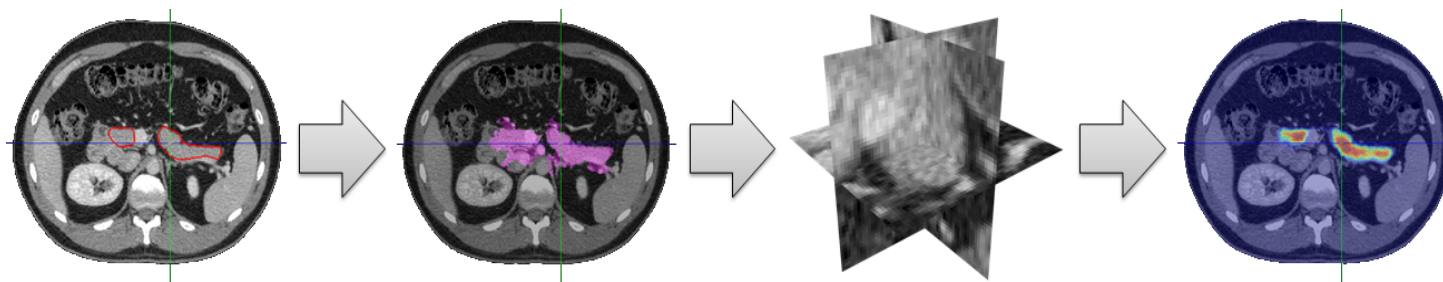
MICCAI 2017 YSA runner-up



A Roadmap of Bottom-up Deep Pancreas Segmentation: from Image Patch, Region, to Holistically-nested CNNs (HNN), P-HNN, Convolutional LSTM (context), ...



ISTP Fellow,
2012-2014



P-ConvNet

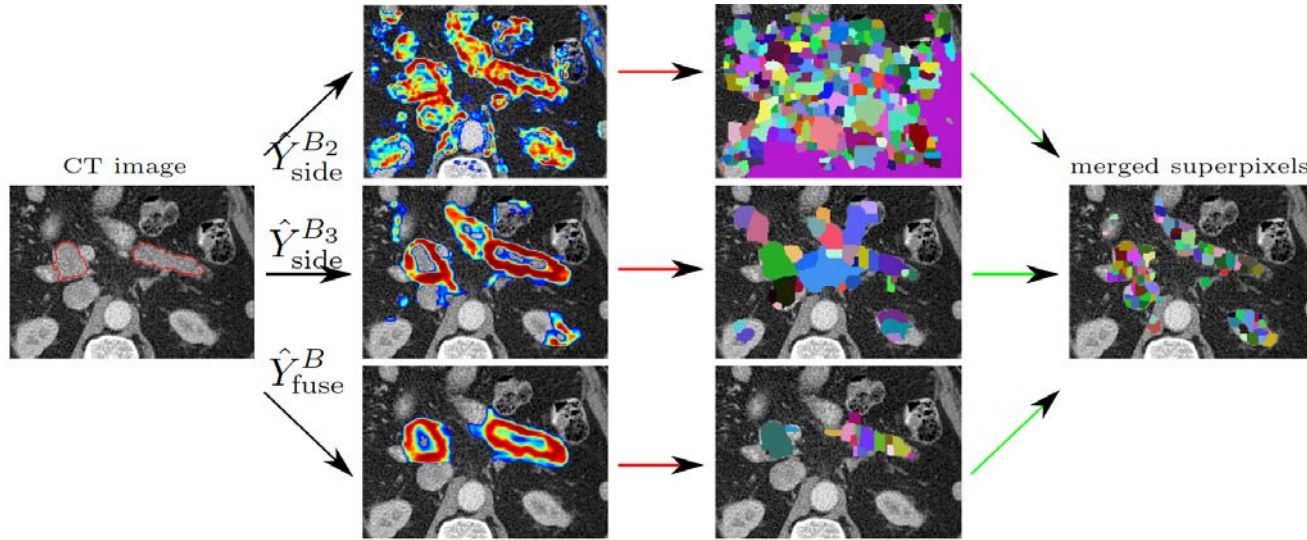
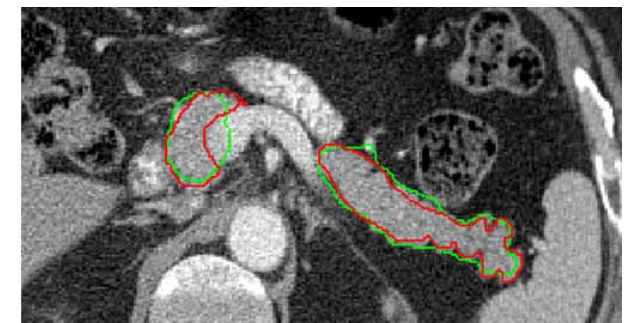
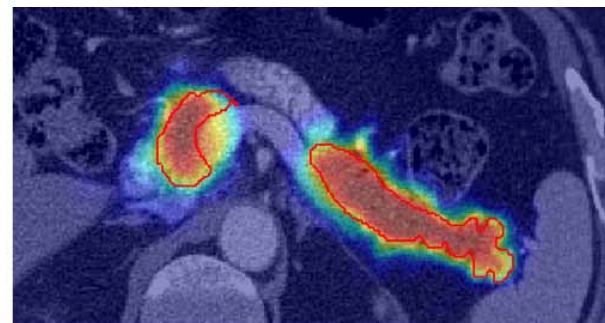
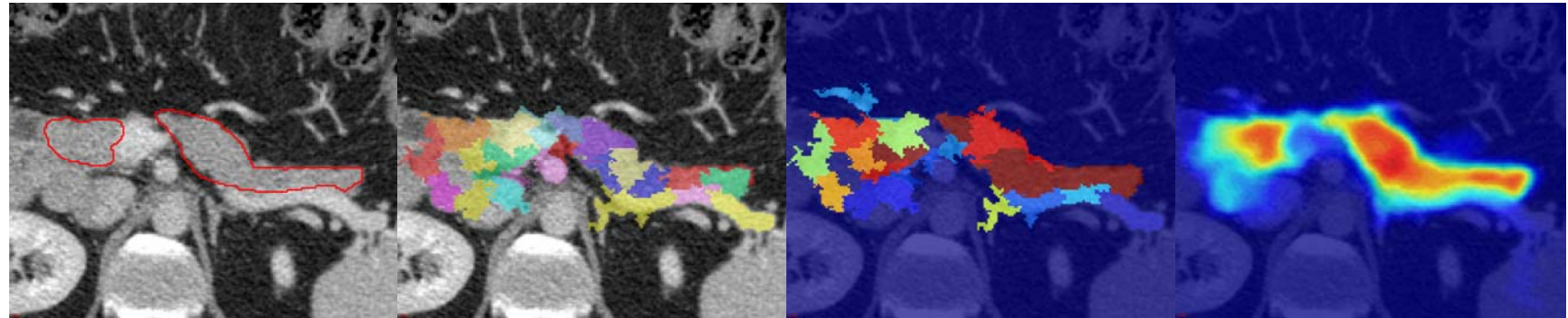


Fig. 2: “Multiscale Combinatorial Grouping” (MCG) [16] on three different scales of learned boundary predication maps from **HNN-B**: $\hat{Y}_{\text{side}}^{B_2}$, $\hat{Y}_{\text{side}}^{B_3}$, and \hat{Y}_{fuse}^B using the original CT image as input (shown with ground truth delineation of pancreas). MCG computes superpixels at each scale and produces a set of merged superpixel-based object proposals. We only visualize the boundary probabilities $p > 10\%$.

Improved pancreas segmentation accuracy over previous state-of-the-art work in Dice coefficients: from 50~60% to ~84%; ASD: from 5~6mm to 0.7mm; computational time from 3 hours to <2 minutes!

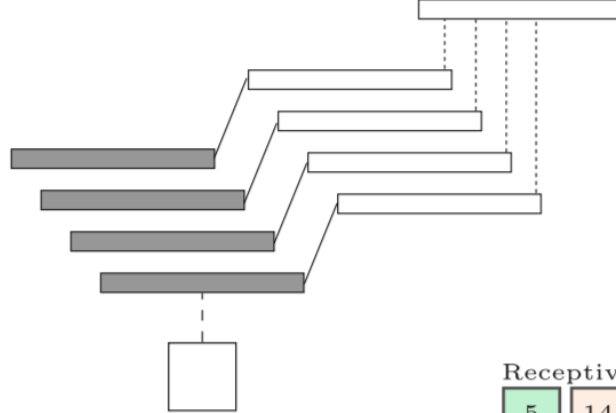


a)

b)

c)

H. Roth, et al., DeepOrgan: Multi-level Deep Convolutional Networks for Automated Pancreas Segmentation. MICCAI (I) 2015: 556-564



(a)

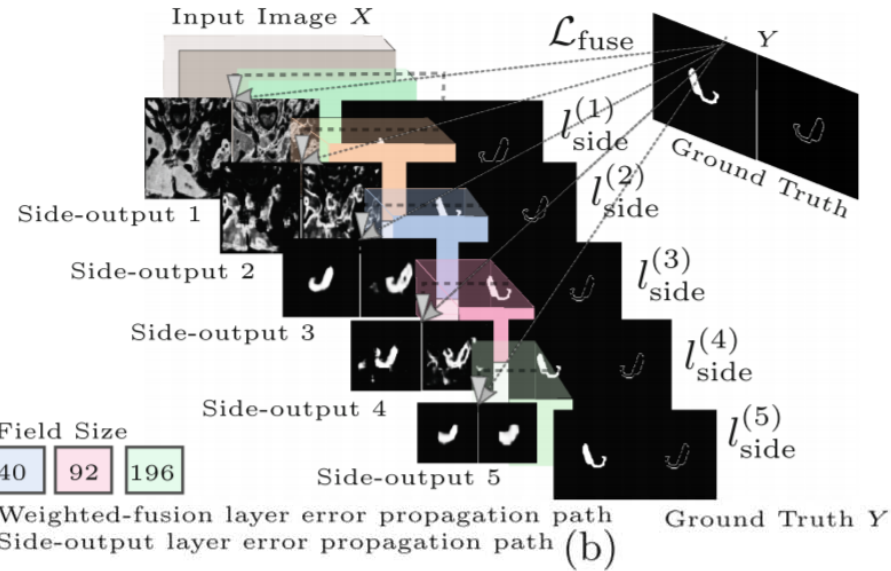
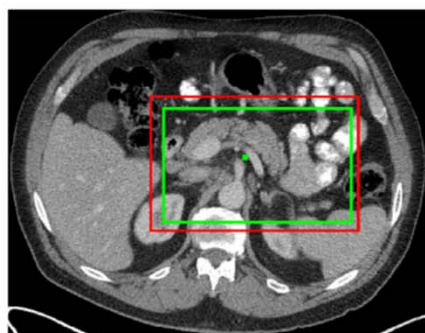


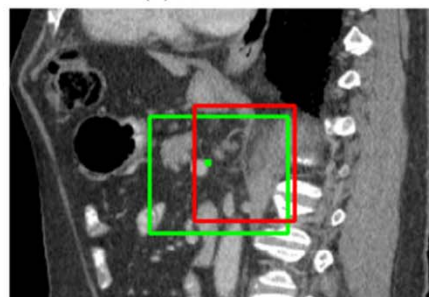
Fig. 1. Schematics of (a) the holistically-nested nets, in which multiple side outputs are added, and (b) the **HNN-I/B** network architecture for both interior (left images) and boundary (right images) detection pathways. We highlight the error back-propagation paths to illustrate the deep supervision performed at each side-output layer after the corresponding convolutional layer. As the side-outputs become smaller, the receptive field sizes get larger. This allows HNN to combine multi-scale and multi-level outputs in a learned weighted fusion layer (Figures adapted from [11] with permission).



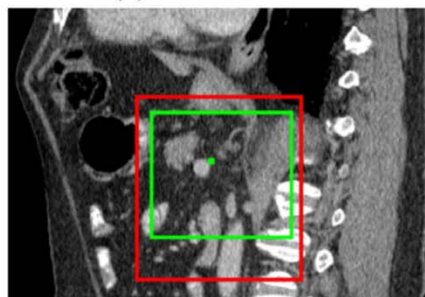
(a) RF: Axial



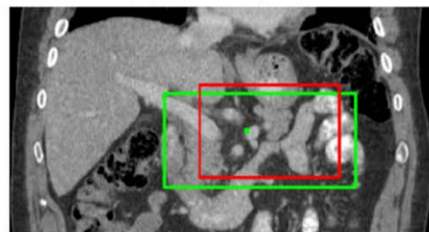
(d) HNN-I: Axial



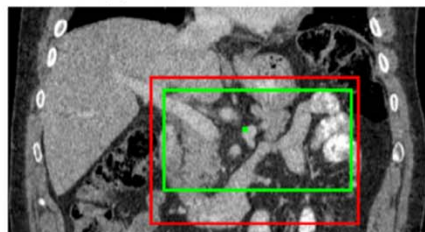
(b) RF: Sagittal



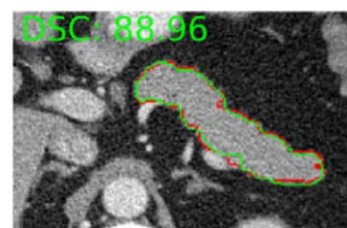
(e) HNN-I: Sagittal



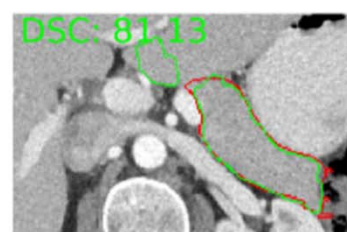
(c) RF: Coronal



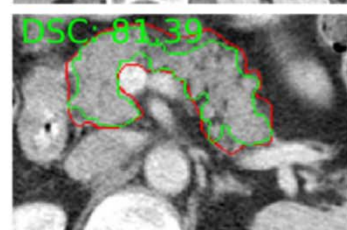
(f) HNN-I: Coronal



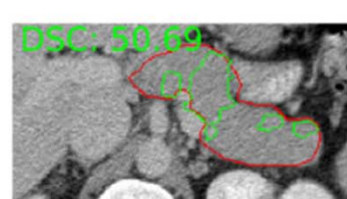
(a)



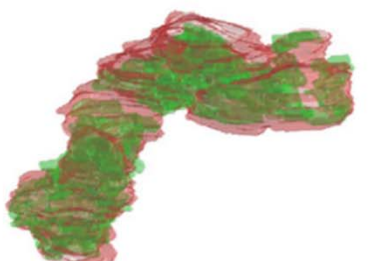
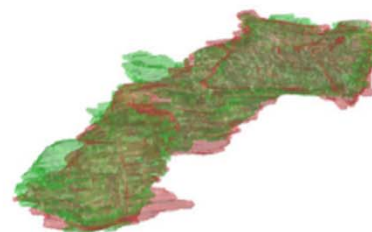
(c)



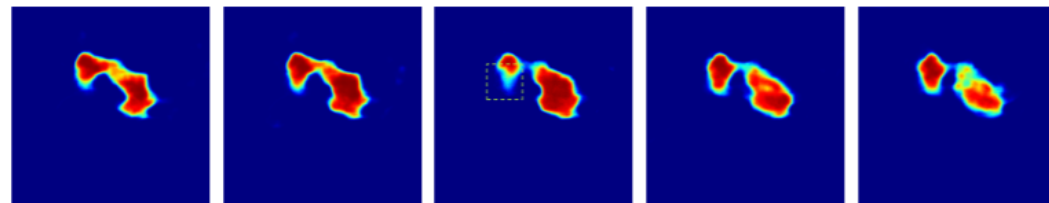
(b)



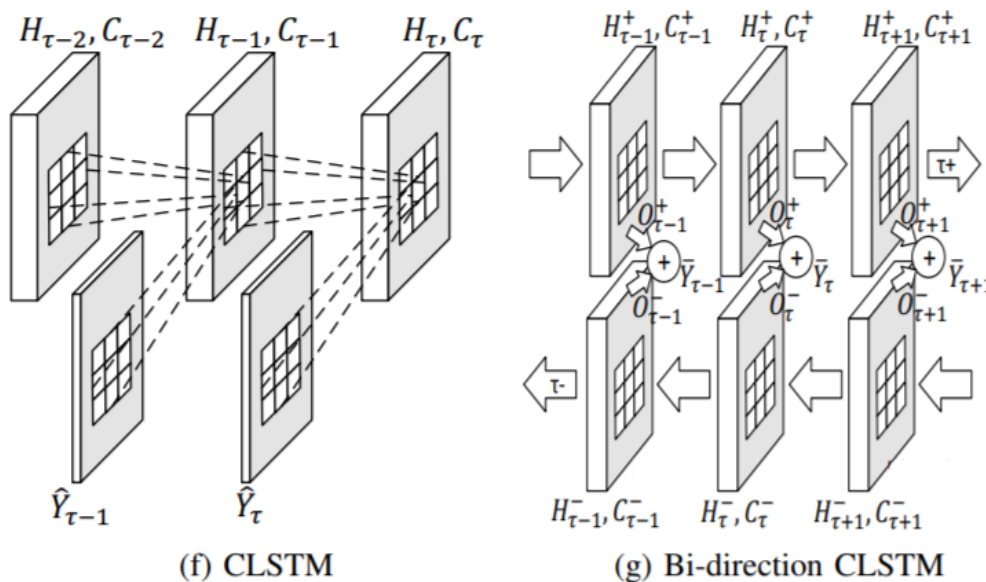
(d)



H. Roth, et al., Spatial aggregation of holistically-nested convolutional neural networks for automated pancreas localization and segmentation, Medical Image Analysis, 45 (2018) 94–107



(a) $\hat{Y}_{\tau-2}$ (b) $\hat{Y}_{\tau-1}$ (c) \hat{Y}_τ (d) $\hat{Y}_{\tau+1}$ (e) $\hat{Y}_{\tau+2}$



(h) $\bar{Y}_{\tau-2}$ (i) $\bar{Y}_{\tau-1}$ (j) \bar{Y}_τ (k) $\bar{Y}_{\tau+1}$ (l) $\bar{Y}_{\tau+2}$

Fig. 4: The main construction units of the proposed RNN sub-network and its input/output segmentation sequence. The sequence of CNN sub-network outputs is shown in the first row (a-e), is taken as the input of the bi-direction CLSTM (g), which is an RNN architecture composed of 2 layers of CLSTM (f) working in opposite directions. The third row (h-l) presents the corresponding output sequence, which is sharp and clean. Note that the missing pancreatic part in \hat{Y}_τ (c), in the green dashed box, is recovered by shape continuity modeling in \bar{Y}_τ (j). For visual clarity, we omit the input $\hat{Y}_{(\cdot)}$ in the bi-direction CLSTM (g), which is same as in (f).

J. Cai, et al., **Pancreas Segmentation in CT and MRI Images via Domain Specific Network Designing and Recurrent Neural Contextual Learning**, MICCAI 2017 <https://arxiv.org/abs/1803.11303>

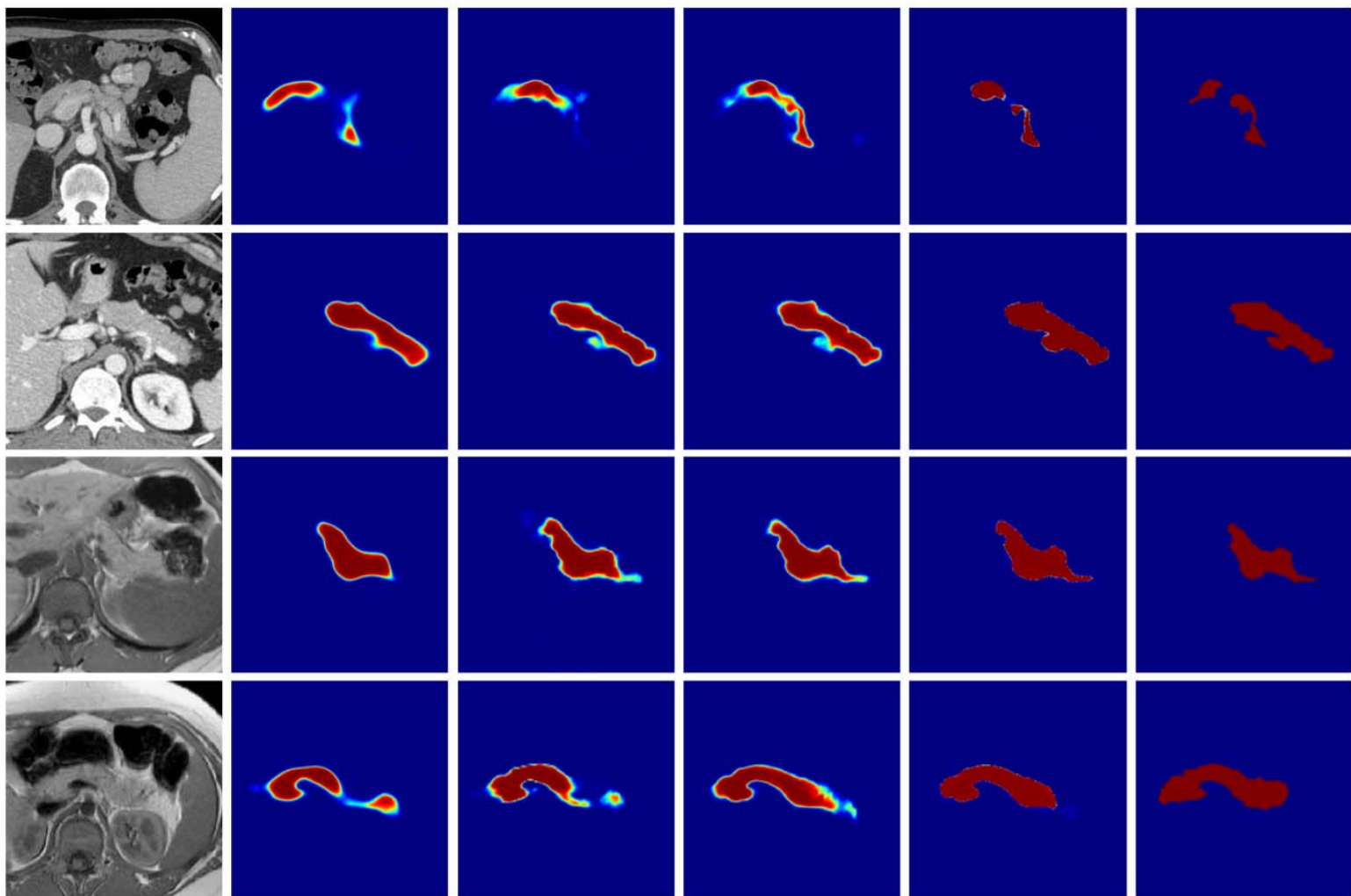


Fig. 8: Examples of output probability map: columns from left to right are the input CT/MRI image, results from HNN [12], UNET [16], the proposed PNet-MSA sub-network, and the full CNN-RNN (“PNet-MSA+BiRNN”), and the ground truth. Our model delivers the most clear probability maps which preserve detailed pancreatic boundaries.

Three Key Problems (III)

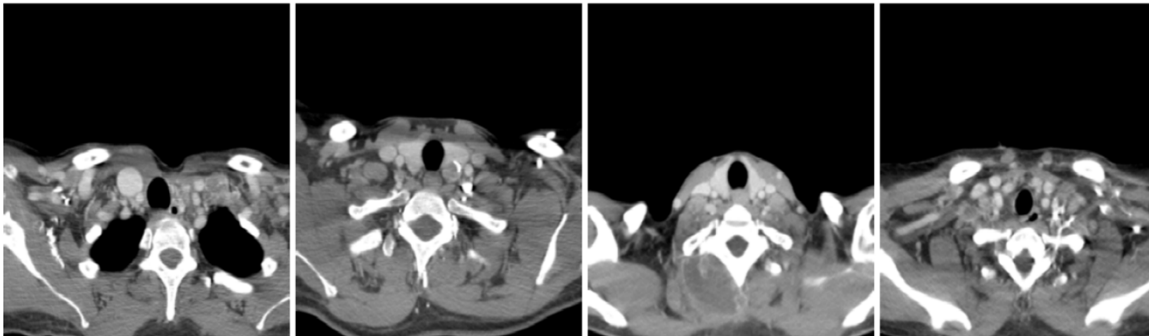
Interleaved or Joint Text/Image Deep Mining at large unconstrained environment or data sources → “big data, weak labels” (~216K 2D key image slices extracted from >60K unique patient studies)

- Interleaved Text/Image Deep Mining on a Large-Scale Radiology Image Database (IEEE CVPR **2015**, a proof of concept study)
- Interleaved Text/Image Deep Mining on a Large-Scale Radiology Image Database for Automated Image Interpretation (its extension, JMLR, 17(107):1–31, **2016**)
- Learning to Read Chest X-Rays: Recurrent Neural Cascade Model for Automated Image Annotation, (IEEE CVPR **2016**)
- Unsupervised Category Discovery via Looped Deep Pseudo-Task Optimization Using a Large Scale Radiology Image Database, IEEE WACV **2017**, **RSNA 2016 Best paper Award**
- ChestX-ray8: Hospital-scale Chest X-ray Database and Benchmarks on Weakly-Supervised Classification and Localization of Common Thorax Diseases, IEEE CVPR **2017**; CVPR **2018**, MICCAI **2018**

➤ **Clinical Impacts:** eventually to build **an automated mechanism** to parse and learn from **hospital scale PACS-RIS databases** to derive semantics and knowledge … has to be *deep learning* based since effective image features are very hard to be hand-crafted cross different diseases, imaging protocols and modalities.

Cluster #5

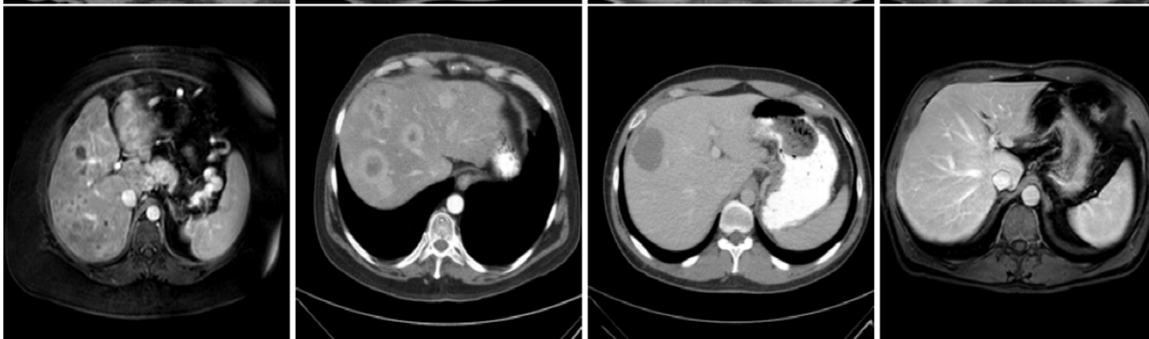
Word	Frequency
neck	656
adenopathy	343
thyroid	295
lymph	292
supraclavicular	236
nodes	218
mass	203
enhancing	96
bulky	77
paratracheal	76



H. Shin, et al., Interleaved Text/Image Deep Mining on a Large-Scale Radiology Image Database, IEEE [CVPR 2015](#)

Cluster #23

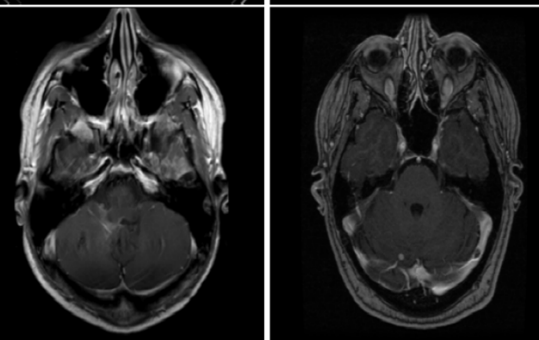
Word	Frequency
liver	524
abdomen	337
enhancement	217
mass	198
lesion	168
lobe	161
adenopathy	119
lesions	109
segment	58
bulky	45



H. Shin, et al., Interleaved Text/Image Deep Mining on a Large-Scale Radiology Image Database for Automated Image Interpretation, [Journal of Machine Learning Research](#), 17(107):1–31, 2016

Cluster #64

Word	Frequency
enhancement	277
cerebellar	193
lesion	192
lobe	186
flair	173
hemisphere	155
mass	134
abnormal	119
frontal	115
cerebellum	113



X. Wang, et al., Unsupervised Joint Mining of Deep Features and Image Labels for Large-Scale Radiology Image Categorization and Scene Recognition, IEEE [WACV 2017](#), <https://arxiv.org/abs/1701.06599>

RSNA 2016, Best Paper Award in (Imaging) Informatics Category!

Learning to Read Chest X-ray using Deep Neural Networks (a little more like humans' interpretation?) [Shin et al., IEEE CVPR 2016]

Lung diseases killing 4 million people every year, in comparison to Nearly 1.3 million people die in road crashes each year!

Statistics from internet ...

10/28/2018

The screenshot shows a news article from the NVIDIA Accelerated Computing News Center. The title is "Detecting and Labeling Diseases in Chest X-Rays with Deep Learning". It features a chest X-ray image and a portrait of a man. Below the article are three examples of X-ray annotations.

Comments 724 Shares

Detecting and Labeling Diseases in Chest X-Rays with Deep Learning

April 14, 2016

Researchers from the National Institutes of Health in Bethesda, Maryland are using NVIDIA GPUs and **deep learning** to automatically annotate diseases from chest x-rays.

Accelerated by **Tesla GPUs**, the team trained their convolutional neural networks on a publicly available radiology dataset of chest x-rays and reports to describe the characteristics of a disease, such as location, severity and the affected organs.

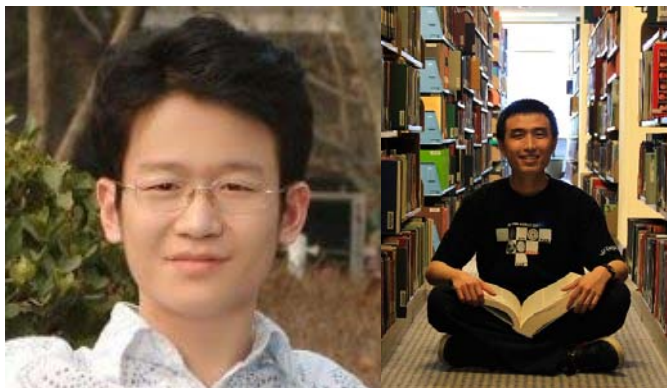
aorta_thoracic / tortuous / mild
aorta_thoracic / tortuous

opacity / lung / middle_lobe / right / aorta_thoracic / tortuous
opacity / lung / base / left

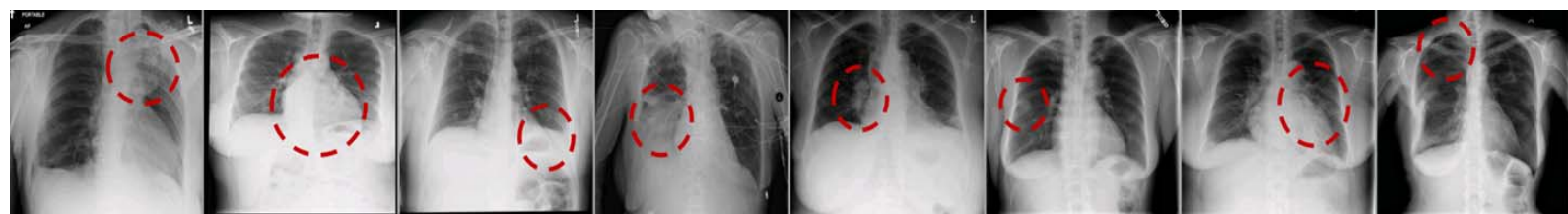
calcified_granuloma / lung / middle_lobe / right / multiple
calcified_granuloma / lung / hilum / right

Examples of annotation generations (light green box) compared to true annotations (yellow box) for input images in the test set.

ChestX-ray8: Hospital-scale Chest X-ray Database and Benchmarks on Weakly-Supervised Classification and Localization of Common Thorax Diseases

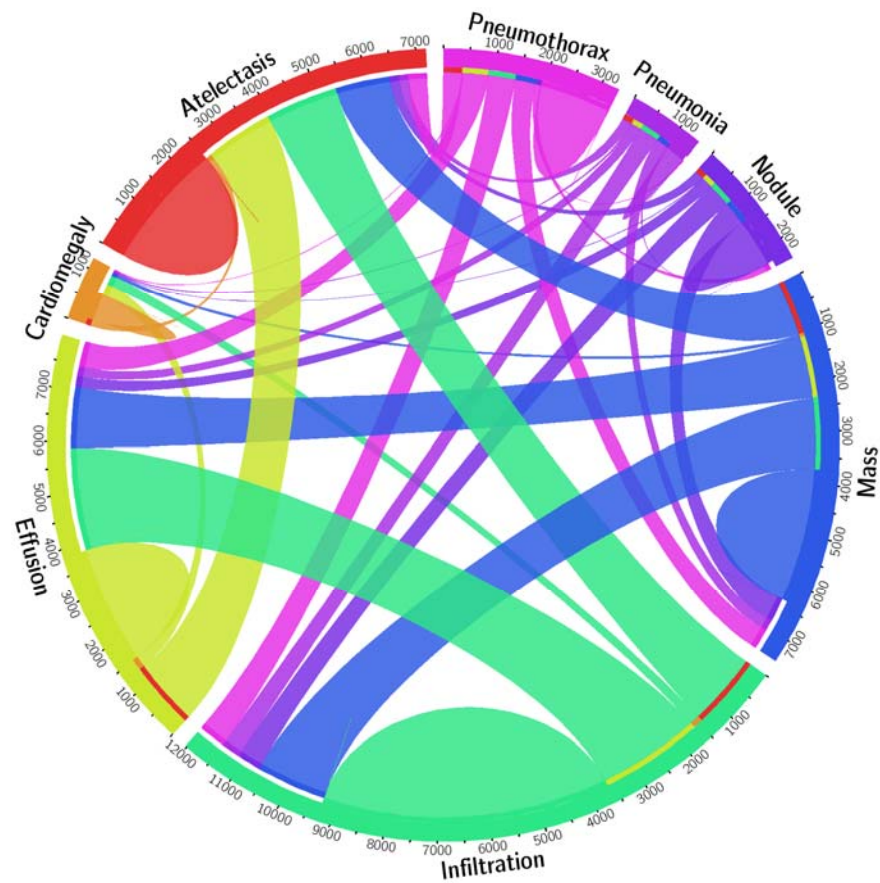


<https://nihcc.app.box.com/v/ChestXray-NIHCC>

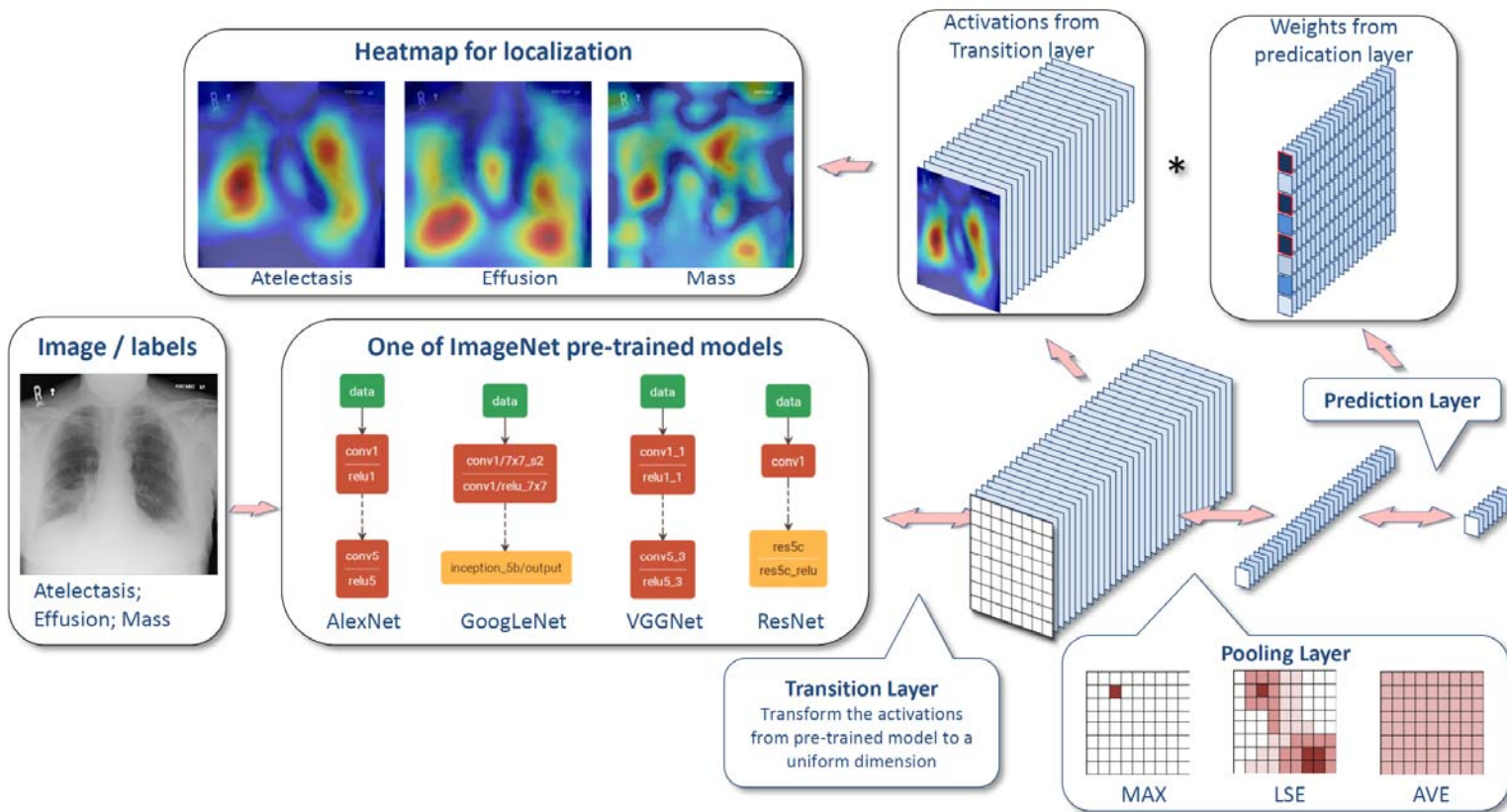


Disease Category Statistics

Item #	OpenI	Ov.	ChestX-ray8	Ov.
Report	2,435	-	108,948	-
Annotations	2,435	-	-	-
Atelectasis	315	122	5,789	3,286
Cardiomegaly	345	100	1,010	475
Effusion	153	94	6,331	4,017
Infiltration	60	45	10,317	4,698
Mass	15	4	6,046	3,432
Nodule	106	18	1,971	1,041
Pneumonia	40	15	1,062	703
Pneumothorax	22	11	2,793	1,403
Normal	1,379	0	84,312	0



Framework Overview



**TieNet: Text-Image Embedding Network
for Common Thorax Disease Classification
and Reporting in Chest X-rays, IEEE
CVPR 2018**

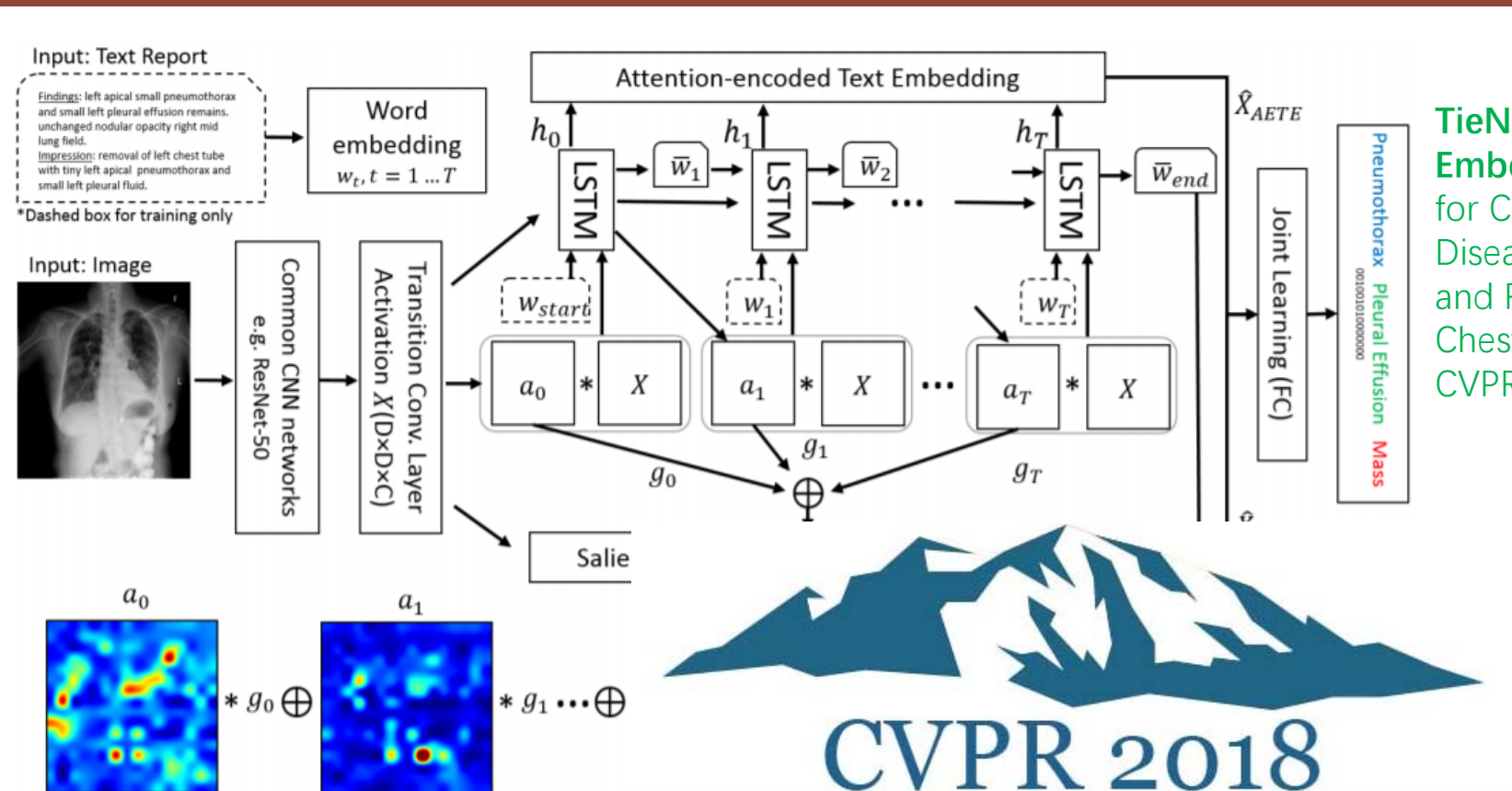
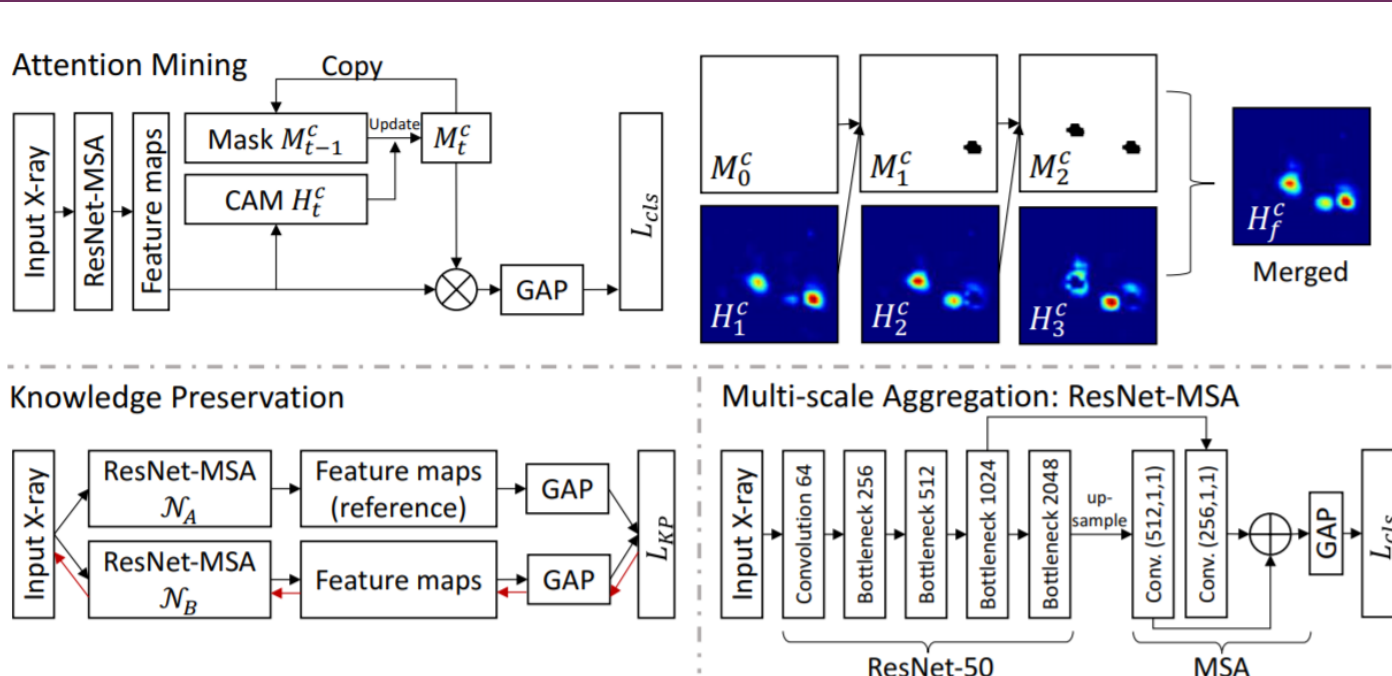


Figure 2. Framework of the proposed chest X-ray auto-annotation system. It takes chest X-ray images and text reports as input to produce saliency-encoded text and image embeddings.

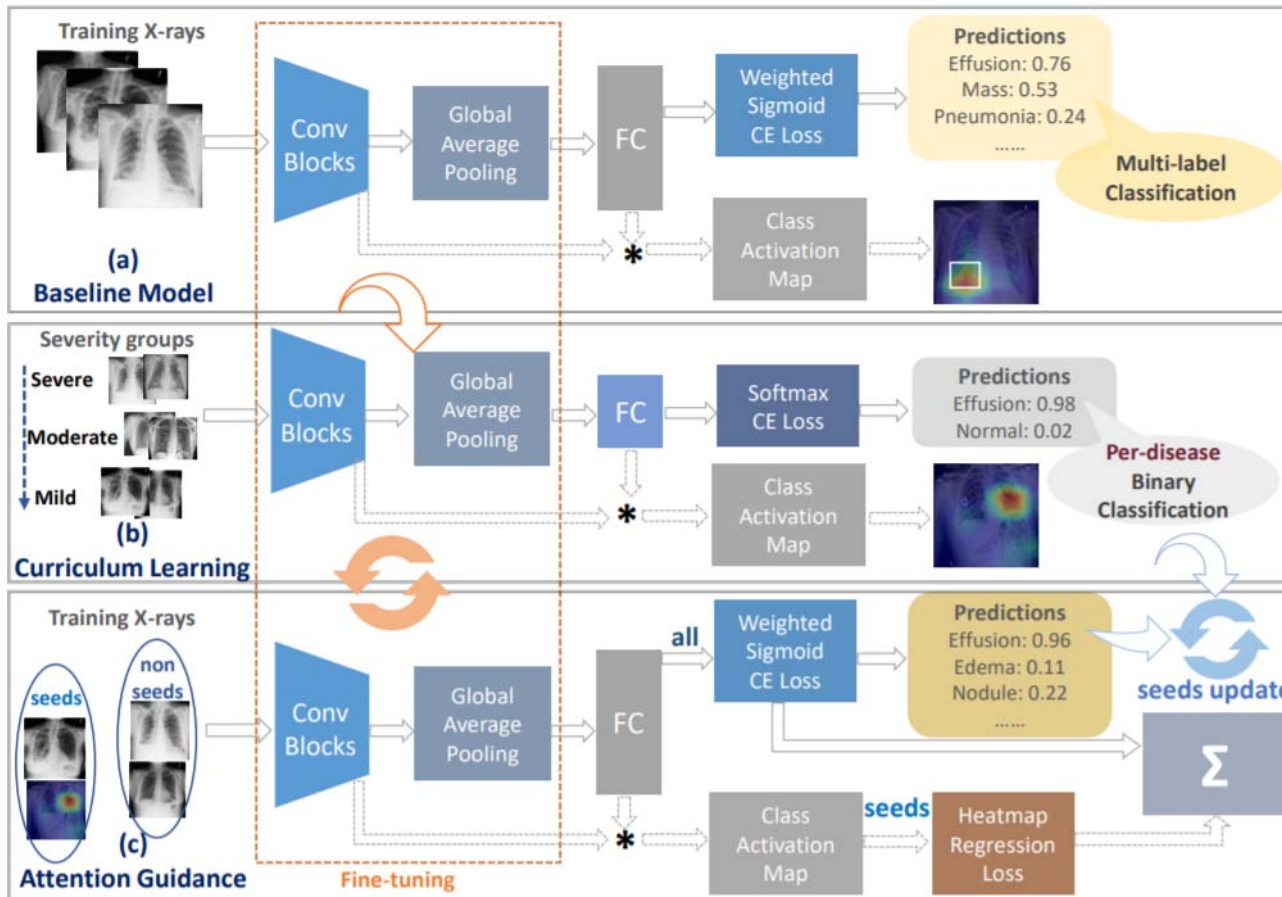
CVPR 2018

Salt Lake City



J. Cai, et al., "Iterative Attention Mining for Weakly Supervised Thoracic Disease Pattern Localization in Chest X-Rays".
MICCAI, 2018,
<https://arxiv.org/abs/1807.00958>,

Fig. 1: Architectures of the proposed attention mining (AM), knowledge preservation (KP), and multi-scale aggregation (MSA). Red arrows in the KP module indicate the path of back-propagation. The convolution parameters for MSA are shown as (number of filters, kernel size, stride). See Sec. 2 for details.



X. Tang, et al., "**Iterative Attention-Guided Curriculum Learning for Weakly Supervised Classification and Localization of Thoracic Diseases on Chest Radiographs**", MLMI, 2018,
<https://arxiv.org/abs/1807.07532>,

Fig. 2. Overall architecture of attention-guided curriculum learning (AGCL).

**Precision Medicine in Oncology → Deep Lesion Graphs in the “Wild”:
Relationship Learning and Organization of Significant Radiology
Image Findings in a Diverse Large-scale Lesion Database**



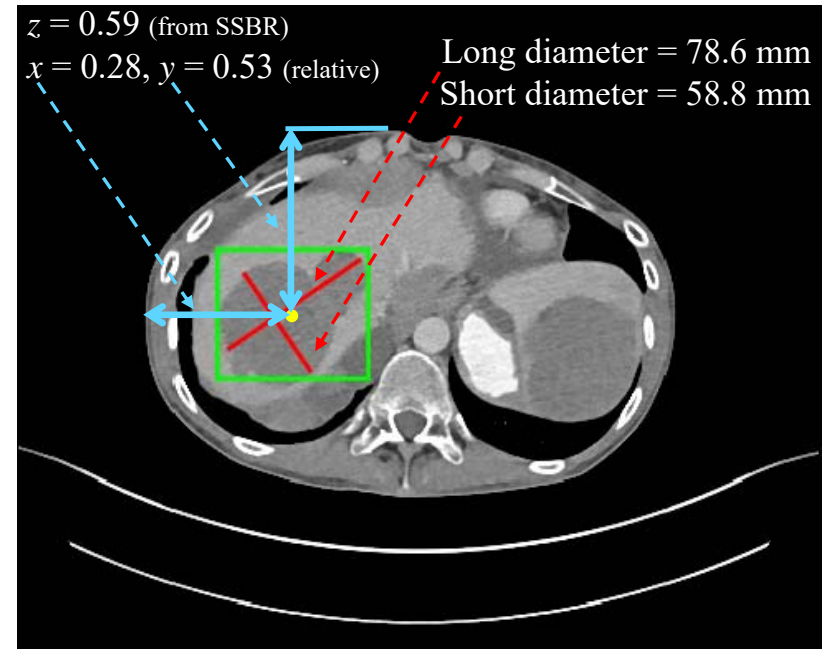
RSNA 2018, Best Paper Award in (Imaging) Informatics Category!

Background

- Large-scale datasets with diverse images and dense annotations are important for both computer vision and medical image
 - Crowd-sourcing can be used in to annotate computer vision datasets, but Medical Imaging requires considerable specialized knowledge & training
 - Mining Internet Images via Deep Learning can be used in computer vision to acquire self-annotations;
- Fortunately, like web data in computer vision, **a vast amount of loosely-labeled and largely untapped data source does exist** in the form of Picture Archiving and Communication Systems (PACS/RIS).
 - Similarly, can we mine the “**unstructured but extremely informative**” PACS?

Background

- Radiologists in their daily work may routinely mark and measure some significant abnormalities or “lesions” on radiology images
 - Collected over years and stored in hospitals’ PACS/RIS
 - Sometime known as “**bookmarks**”
 - Used to assess patients’ conditions or therapy responses

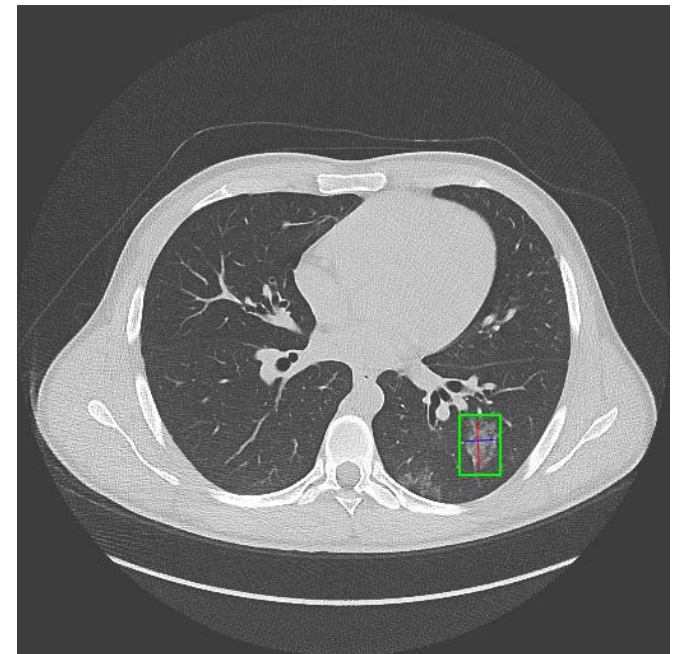


To the best of our knowledge, no prior work has been done on **learning “deep lesion” similarity graph & embedding** via imaging on such a **“large-scale”** comprehensive dataset with **“weak”** cues!

DeepLesion Database

<https://nihcc.app.box.com/v/DeepLesion>

- Mined from bookmarks (RECIST diameters) in NIH's PACS
- 32,120 axial CT slices from 10,594 studies of 4,427 unique patients; ~900K CT slices total
- 1–3 lesions in each image with size measurements (long-axis and short axis)
- 32,735 lesions altogether
- Convert any pair of diameters to a bounding-boxes
 - $(x_{min} - 5, y_{min} - 5, x_{max} + 5, y_{max} + 5)$
 - $x_{min} = \min(x_{11}, x_{12}, x_{21}, x_{22}),$
 - $x_{max} = \max(x_{11}, x_{12}, x_{21}, x_{22})$



Problem Definition

- Lesions in DeepLesion are **basically unsorted and lack semantic labels**, *e.g.*, lung nodule, mediastinal lymph node
- Our goal: understand and organize a large quantity of lesions, or oncology findings, by “**Automated Instance-level Similarity Modeling & Topology-discovery Mining**”
 1. discover **their types and locations**
 2. find similar lesions from a population of different patients, *i.e.*, **content-based retrieval**
 3. track the same lesions within the same patient’s several longitudinal studies, *i.e.*, lesion instance **matching or tracking** among multiple studies
<https://www.healthdatamanagement.com/news/oncology-ai-runs-on-the-arterys-mica-medical-imaging-cloud-ai-platform>
- Our approach: learning “**functional**” deep feature representations for each instance that capture & keep the similarity relationship in **type**, **location**, and **size**, etc.
- **Scientifically-viable, practical** approaches on doing such AI/DL medical imaging task at scale! → precision imaging measurements for oncology ...

Related Work

- **Deep Metric Learning**
 - **Siamese network** [1]
 - **Triplet network** – “weak deep learning, or DL with **weak data self-regularization!**”
$$\|f(A) - f(P)\|_2^2 + m < \|f(A) - f(N)\|_2^2$$
- **Triplet Loss** with multiple labels with hierarchical structures [2]
 - Our method shares the similar spirit with [2], but we **lack well-defined supervision cues (to define which pair is more similar than the other, and logically why?)** given the significant radiology findings in the collected dataset
 - We proposed strategies to propose and leverage **weak cues**, e.g., self-supervised body part regressor and iterative refinement, etc.

[1] J. Bromley et al. Signature verification using a “siamese” time delay neural network, NIPS 1994

[2] X. Zhang et al. Embedding label structures for fine-grained feature representation, CVPR 2016

Related Work

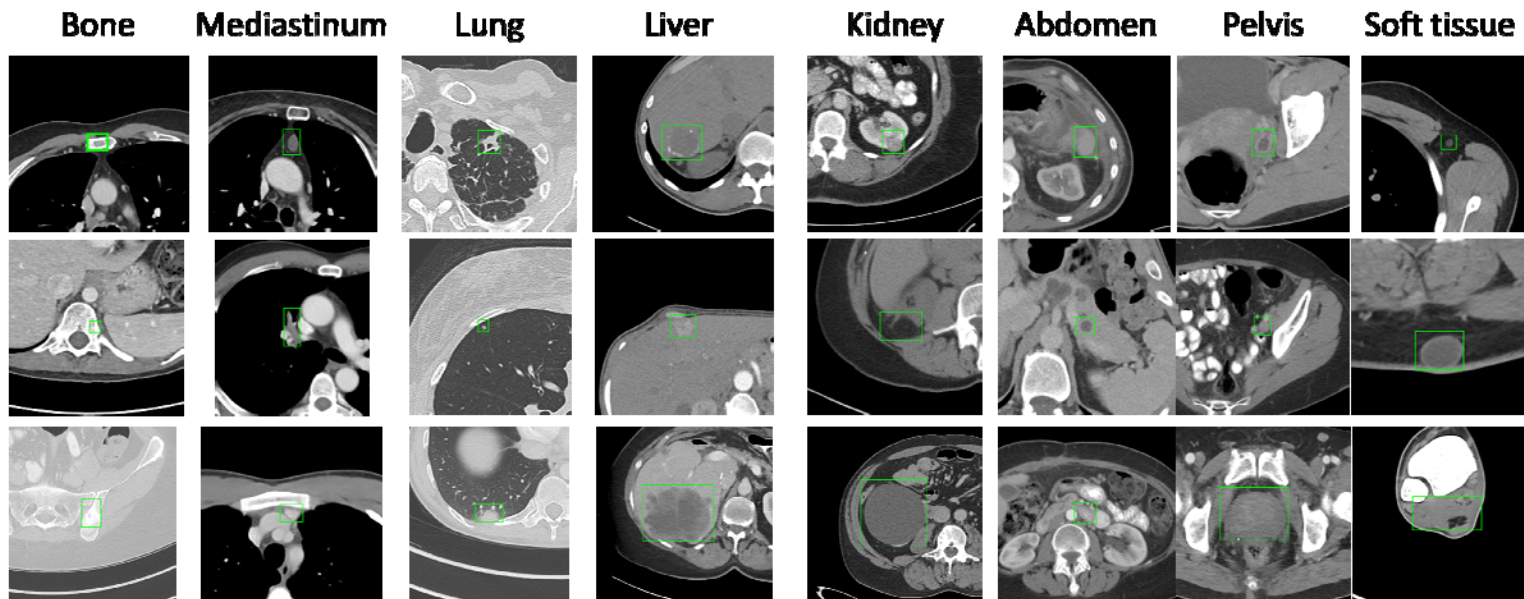
- **Lesion Retrieval (inter-patients)**
 - Existing methods typically focus on **one type of lesion** (e.g., lung lesion or mammographic mass) and learn the similarity relationship based on **fully manually-annotated labels** (or radiology reports)
 - We learn deep lesion embedding on a large diverse dataset with **weak cues**, in a **self-regularization** manner when “**big data**” are available!
- **Lesion Matching** (across **intra-patient** multiple time points)
 - Existing work generally require organ segmentation or time-consuming non-rigid volumetric registration and focus on certain lesion types
 - Our lesion embedding is fast and can match **all “categories” of lesions**

Liu, Lu, Ye, Yu, Huang: Coarse-to-fine classification via parametric and **nonparametric models for computer-aided diagnosis**. ACM CIKM 2011

Bi, Wu, Lu, Liu, Tao, Wolf: AdaBoost on **low-rank PSD matrices for metric learning**. IEEE CVPR 2011

Supervision Cue (I): Lesion Type

- We randomly select 30% lesions and manually label them into **8 types**: lung, abdomen, mediastinum, liver, pelvis, soft tissue, kidney, and bone
 - Coarse-scale attributes of the lesions



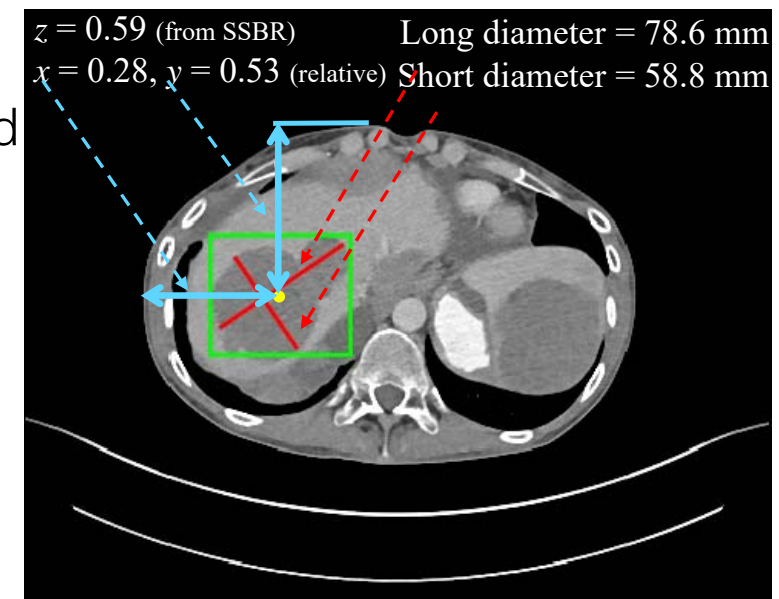
Supervision Cue (I): Lesion Type

- **Mediastinum:** mainly consists of lymph nodes (LNs) in the chest
 - **Abdomen:** miscellaneous ones that are not in liver or kidney
 - **Soft tissue:** lesions and LNs in the muscle, skin, fat, etc.
-
- Among the labeled samples, we randomly select 25% as training seeds to predict pseudo-labels, 25% as the validation set, and the other 50% as the test set
 - We use labeled seed samples to train a classifier (RBF SVM) on ImageNet pre-trained deep image features and apply it to all unlabeled samples to get their **pseudo-labels** (**may be noisy!**)

Supervision Cue (II): Relative Body Location

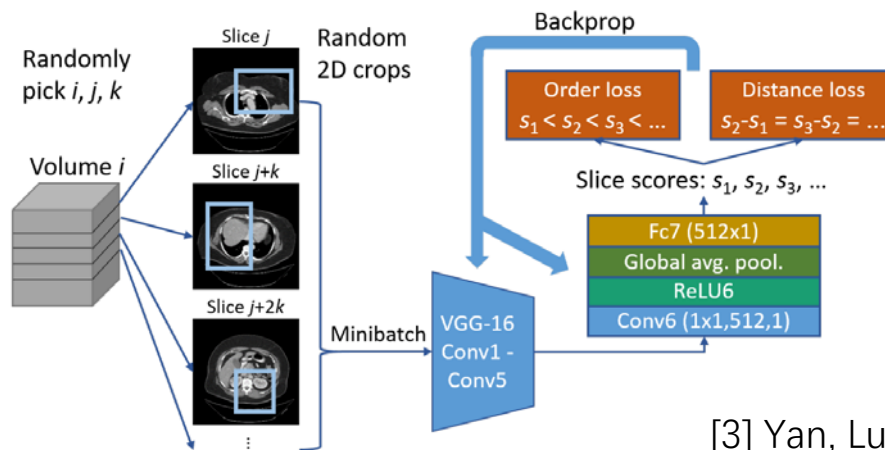
- X and Y : easy ☺
- Z : self-supervised body part regression or regressor (SSBR) [3]
- SSBR [3]
 - Intuition: volumetric medical images are intrinsically Upper/Down structured or ordered
 - The superior-inferior slice order information (self-supervision) can be leveraged to learn an deep appearance-based *z predictor*

[3] Yan, Lu, Summers. Unsupervised Body Part Regression via Spatially Self-ordering Convolutional Neural Networks, ISBI 2018



Supervision Cue (II): Relative Body Location

- h is the sigmoid function, g is the smooth L1 loss
- The **order loss** and **distance loss** terms collaborate to push each slice score towards the correct direction **relative to other slices**



$$\begin{aligned}
 L_{\text{SSBR}} &= L_{\text{order}} + L_{\text{dist}}; \\
 L_{\text{order}} &= - \sum_{i=0}^{m-2} \log h(s_{j+k(i+1)} - s_{j+ki}); \\
 L_{\text{dist}} &= \sum_{i=0}^{m-3} g(\Delta_{i+1} - \Delta_i), \\
 \Delta_i &= s_{j+k(i+1)} - s_{j+ki},
 \end{aligned}$$

[3] Yan, Lu, Summers. Unsupervised Body Part Regression via Spatially Self-ordering Convolutional Neural Networks, ISBI 2018

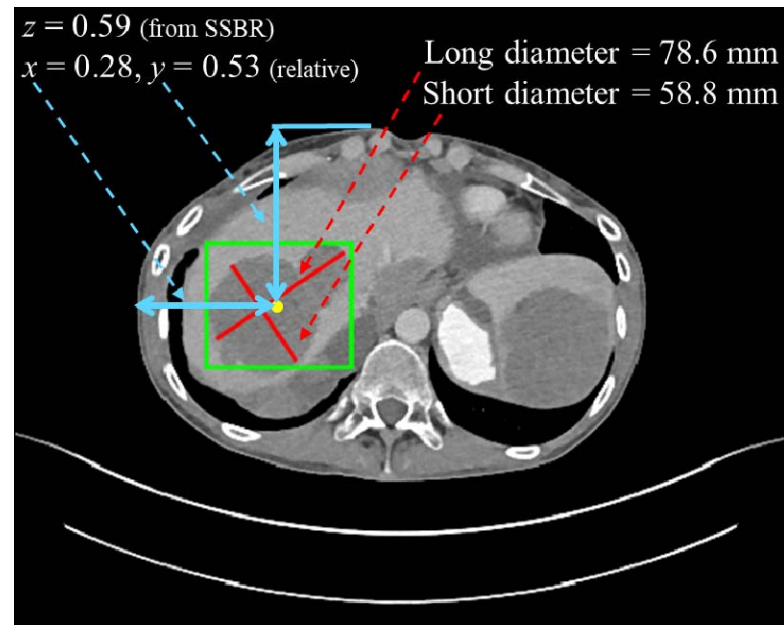
Figure 2. Framework of the self-supervised body part regressor (SSBR).

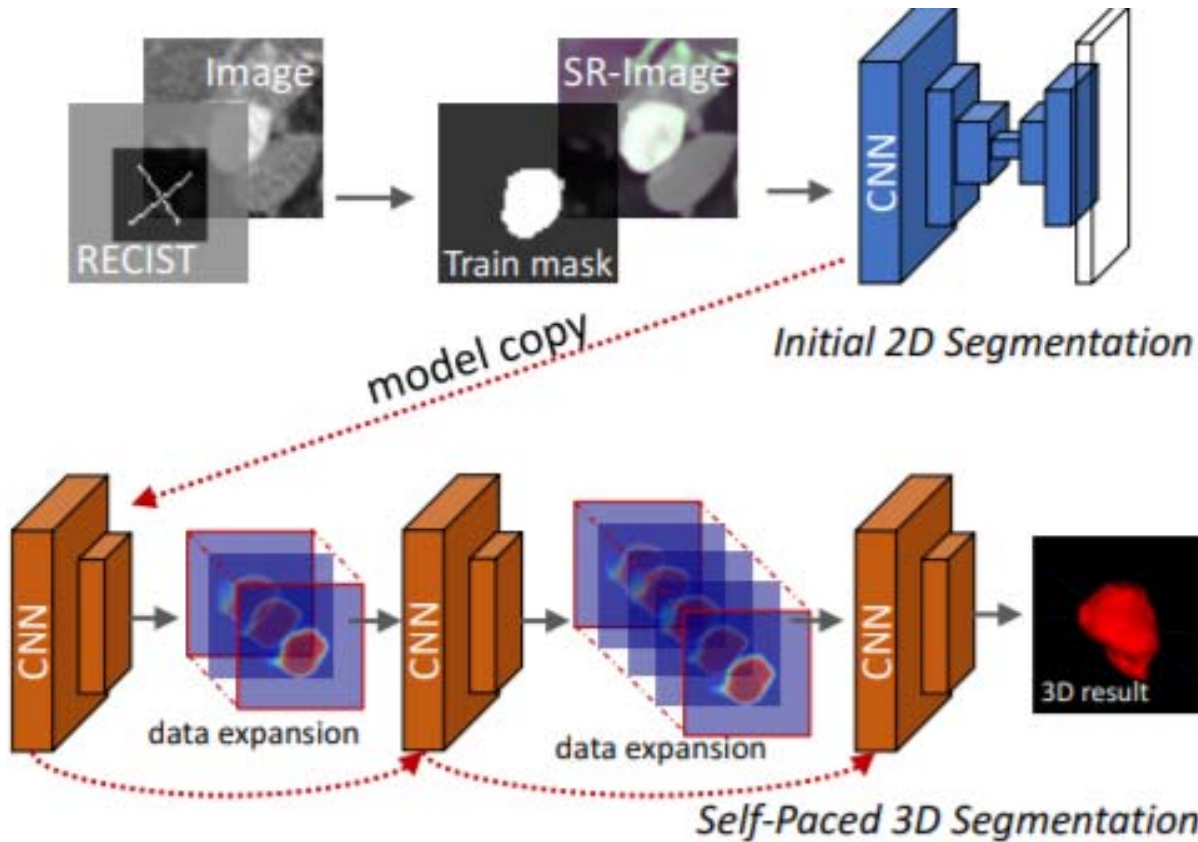
Supervision Cue (II): Relative Body Location

- In DeepLesion, some CT volumes are zoomed in on a portion of the body, *e.g.*, only the left half is shown
 - Technique: train SSBR on **random crops** of the axial slices
- **Data Augmentation:** SSBR does not perform well on **rare body parts** that are much less frequent in the training set, *e.g.*, head and legs → **inconsistency!**
 - Technique: train SSBR → examine the correlation coefficients (γ) of slice scores and slice indices to find rare parts → train SSBR again on a **resampled training set** with **hard** volumes oversampled

Supervision Cue (III): Lesion Size

- Lengths of long and short axes of lesion diameters
- Has already been annotated and measured by radiologists
- Ranges from 0.2 to 343 mm with a median of 15.6 mm





J. Cai, et al., "Accurate Weakly-Supervised Deep Lesion Segmentation using Large-Scale Clinical Annotations: Slice-Propagated 3D Mask Generation from 2D RECIST", MICCAI, 2018, [arXiv:1801.08614](https://arxiv.org/abs/1801.08614),

Figure 1. Overview of the proposed weakly supervised self-paced segmentation with CNN (Sec.3) for 3D lesion segmentation.

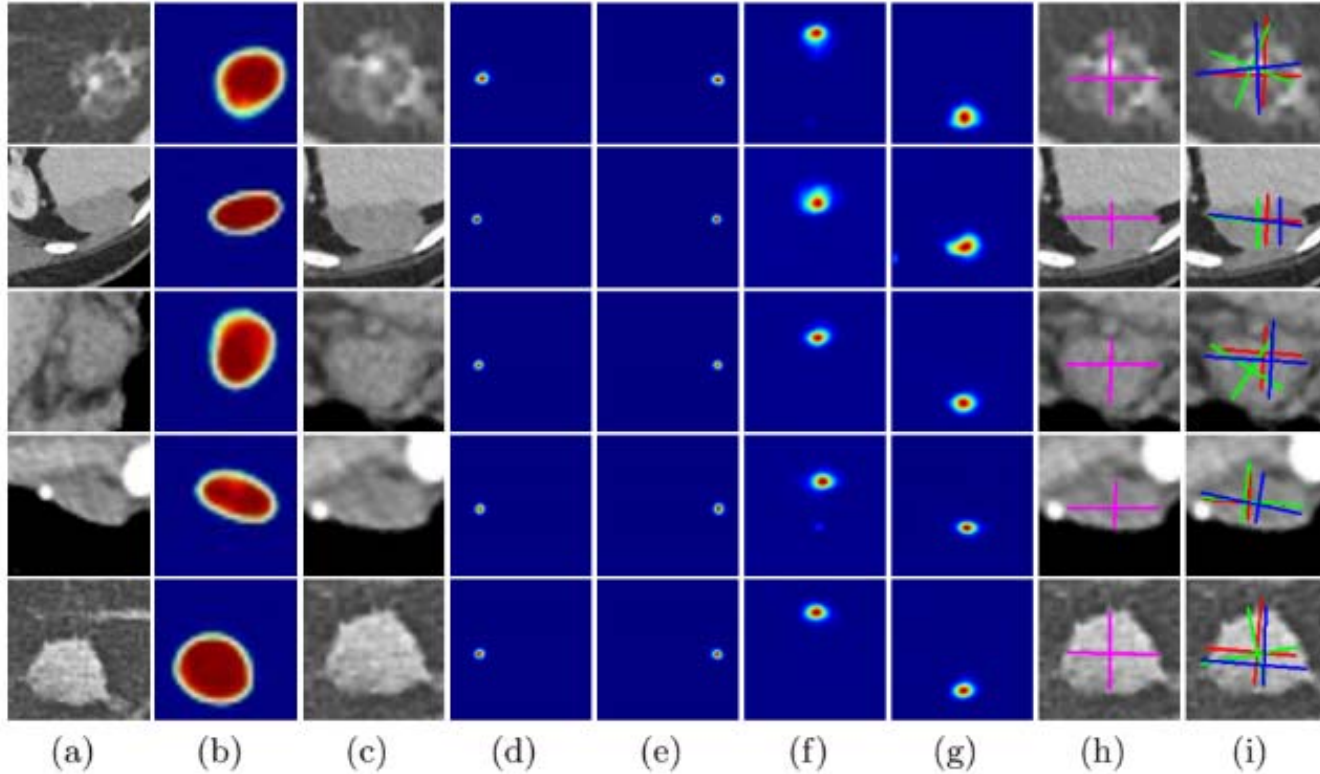
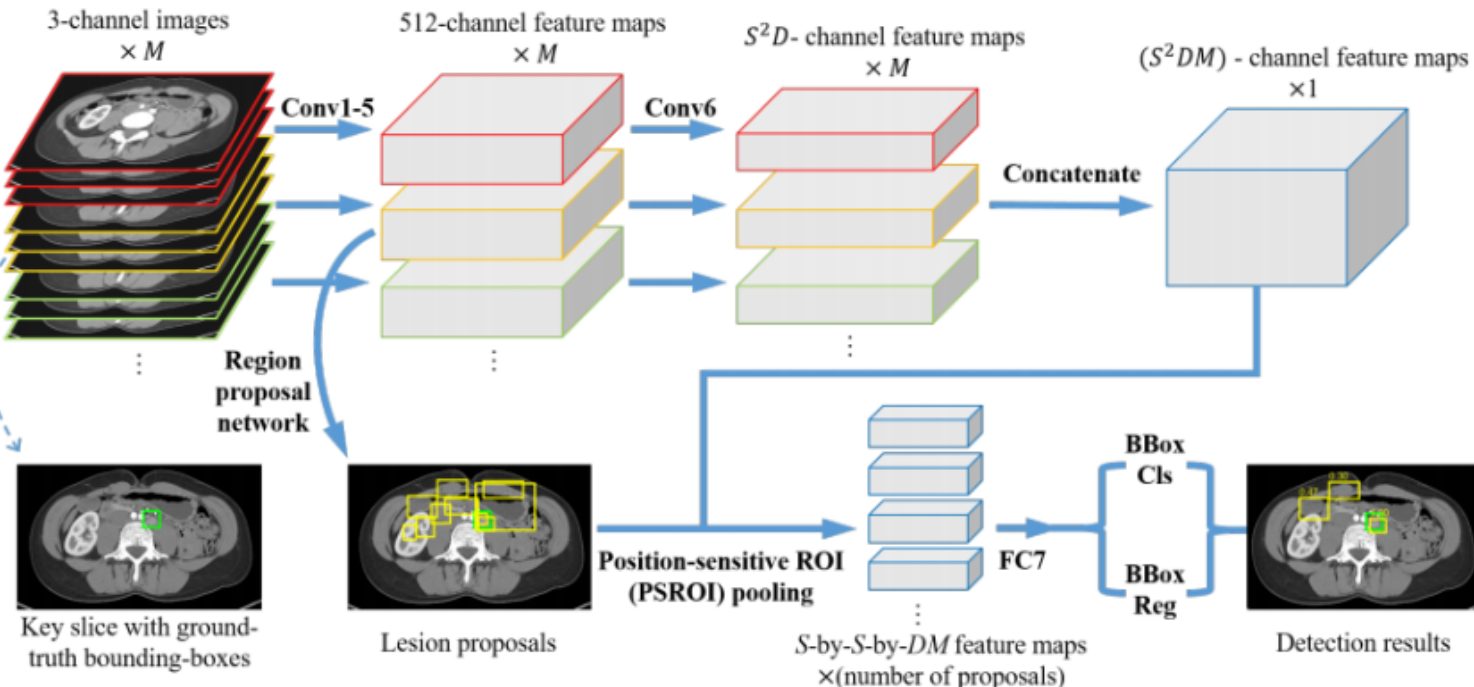


Fig. 3. Given the input test image (a), we can obtain the predicted lesion mask (b), the transformed image (c) from the STN, and the estimated keypoint heatmaps (d)-(g) from the SHN. From (d)-(g), we obtain the estimated RECIST (h), which is close to the annotations (i) labeled by radiologists. Red, green, and blue marks denote DL, R1,

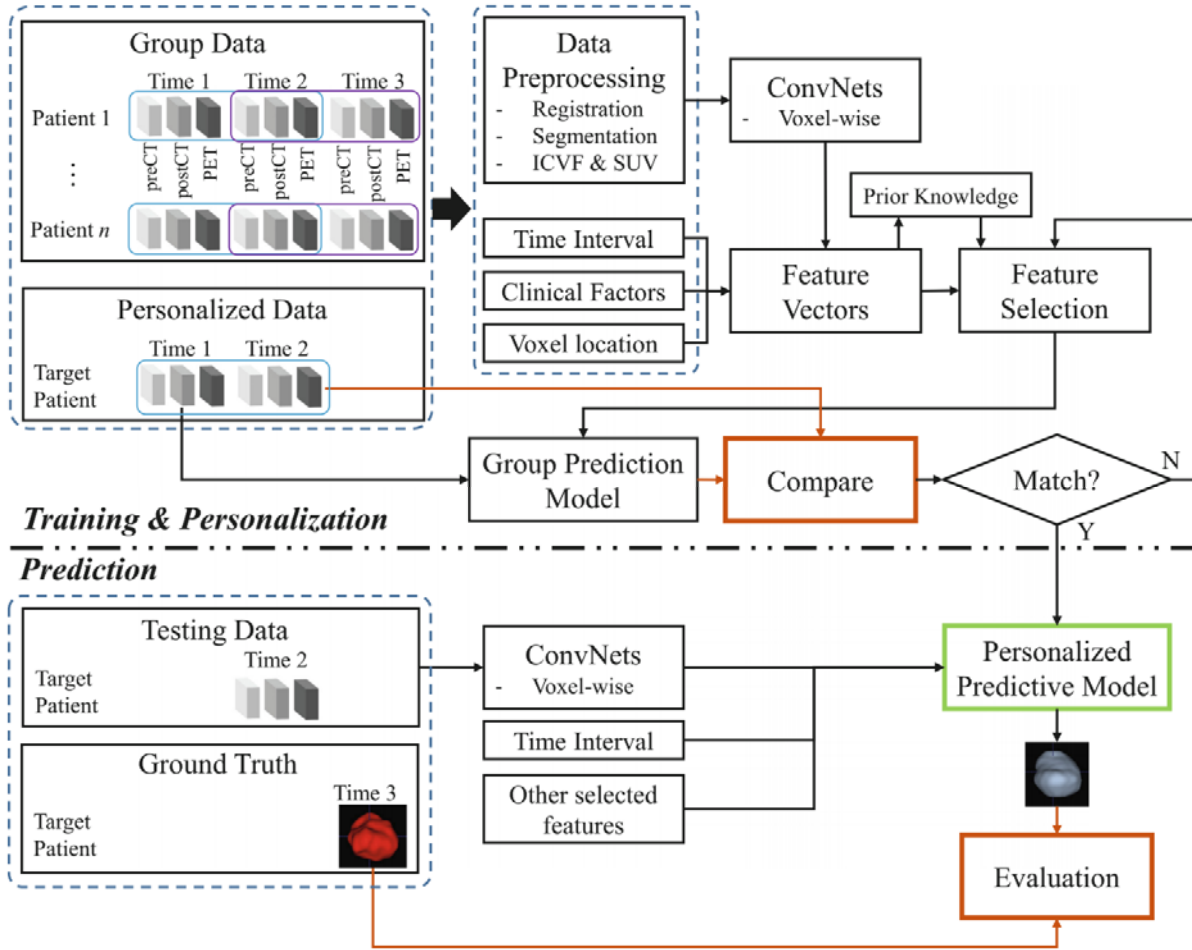


Y. Tang, et al., "Accurate Semi-Automatic RECIST Labeling on CT Scans with Cascaded Convolutional Neural Networks", MICCAI, 2018,

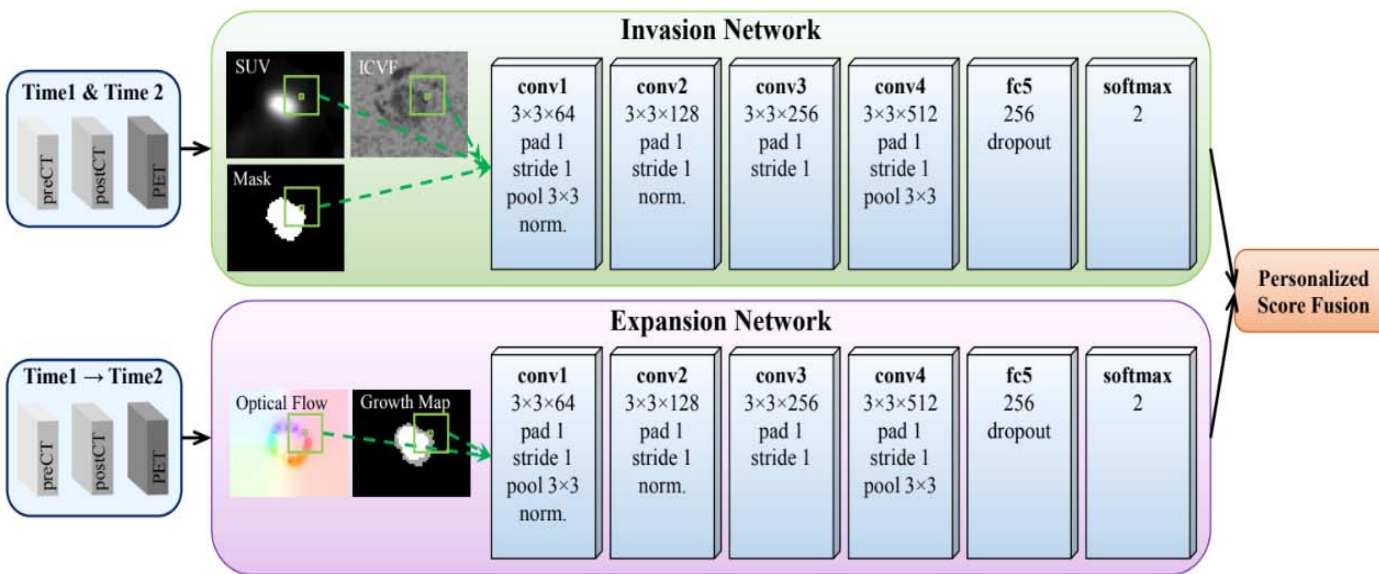


K. Yan, et al., "3D Context Enhanced Region-based Convolutional Neural Network for End-to-End Lesion Detection", MICCAI, 2018,

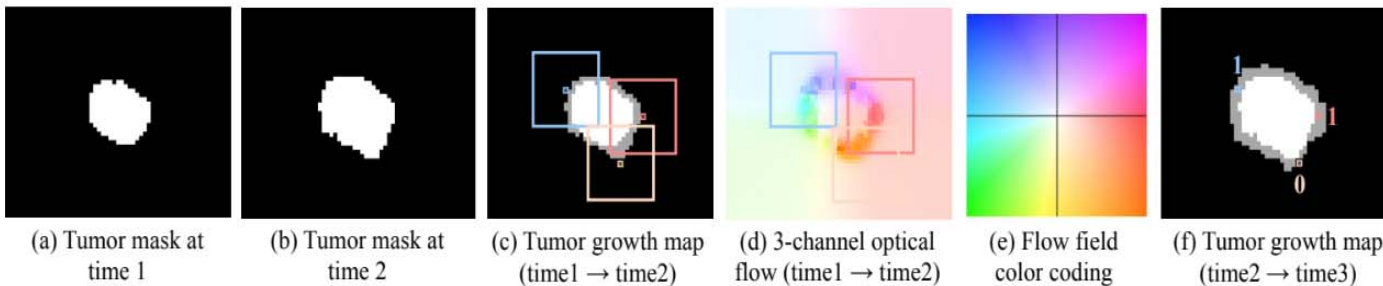
Fig. 1. The framework of 3D context enhanced region-based CNN (3DCE) for lesion detection.



L. Zhang, et al., **Personalized Pancreatic Tumor Growth Prediction via Group Learning**, MICCAI 2017



architecture for late fusion of the invasion and expansion networks for predicting tumor growth.



L. Zhang, et al., Convolutional **Invasion** and **Expansion** Networks for Tumor Growth Prediction, IEEE Trans. Medical Imaging, 2018

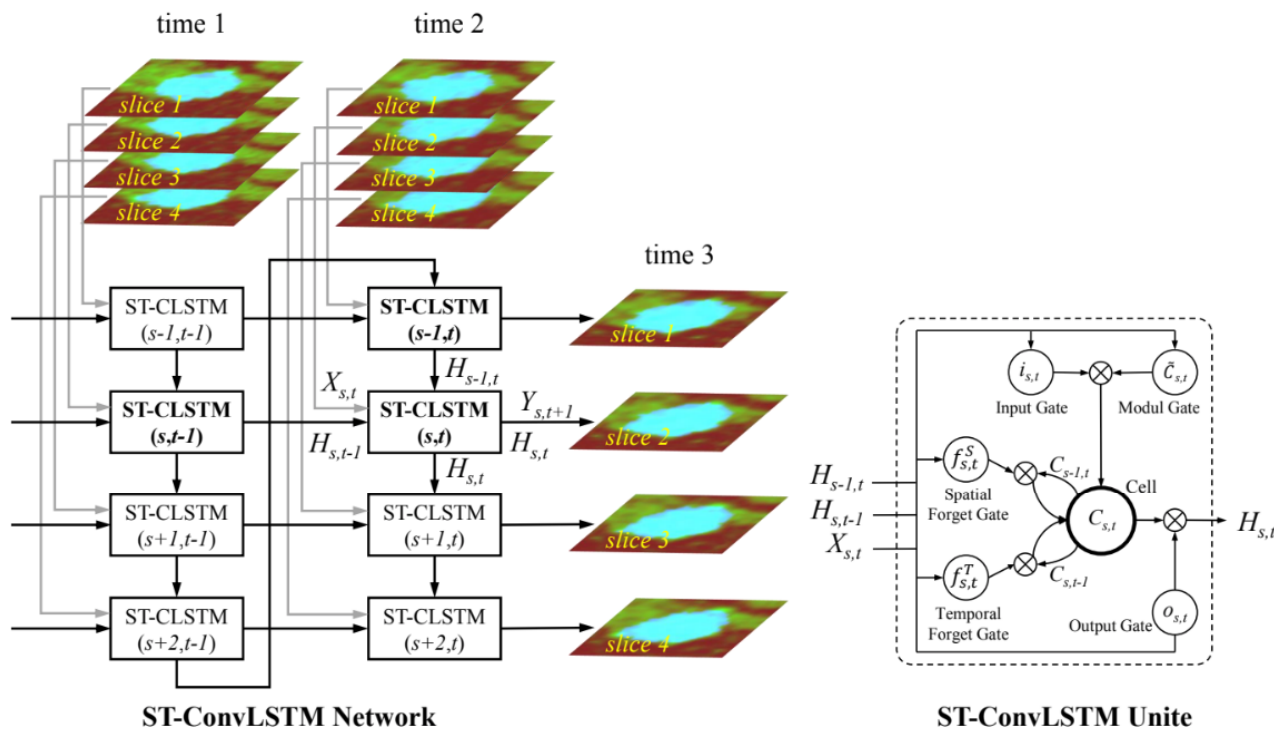


Fig. 1. Left: The proposed Spatial-Temporal Convolutional LSTM (ST-ConvLSTM, or ST-CLSTM) network for learning 4D longitudinal data to predict tumor growth. In this example, 3 time points each with 4 spatially adjacent image slices (each slice is a 3-channel color image) are shown. **Right:** The ST-ConvLSTM unit.



L. Zhang, et al., **Spatial-Temporal Convolutional LSTMs: Learning 4D Longitudinal Data for Tumor Growth Prediction**, 2018

Build Triplet Network with Sequential Sampling

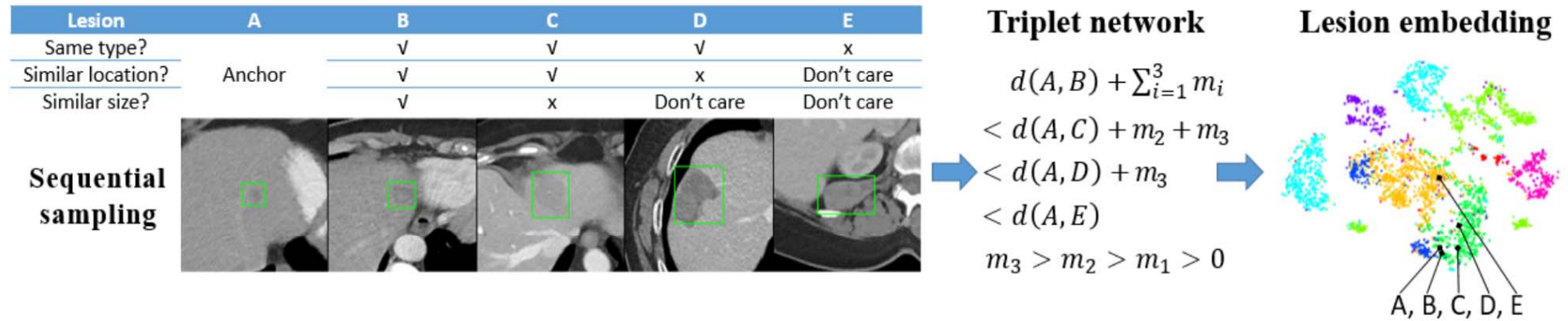


Figure 1. The proposed framework. Using a triplet network, we learn a feature embedding for each lesion in our comprehensive DeepLesion dataset. Training samples A–E are selected with a sequential sampling strategy so as to make the embeddings respects similarity in type, location, and size.

- With a flavor of “**Gibbs Sampling**”; sampling similarity orders according to each **marginal/conditional distribution** (e.g., body location similarity), iteratively → to comply similarity scores into the **joint distribution**
- **“Cue Priorities”, not all cues are created equally!** → DL or DNN is “paradigm shifting” or “super component”?
- **Ranking** a series of samples to make them **self-organize and move to** the right space in the feature space!

Triplet network with Sequential Sampling

- Do not use hard triplet mining because of the noisy cues
- Note that there is label noise in the 4th row of Fig. 3, where lesion D does not have the same type with $A \sim C$ (soft tissue versus pelvis)

$$\|f(A) - f(P)\|_2^2 + m < \|f(A) - f(N)\|_2^2$$

where an anchor A, a positive sample P with the **same label** as A, and a negative sample N with a **different label**. $f(\cdot)$ is the embedding function to be learned and m is a predefined margin.

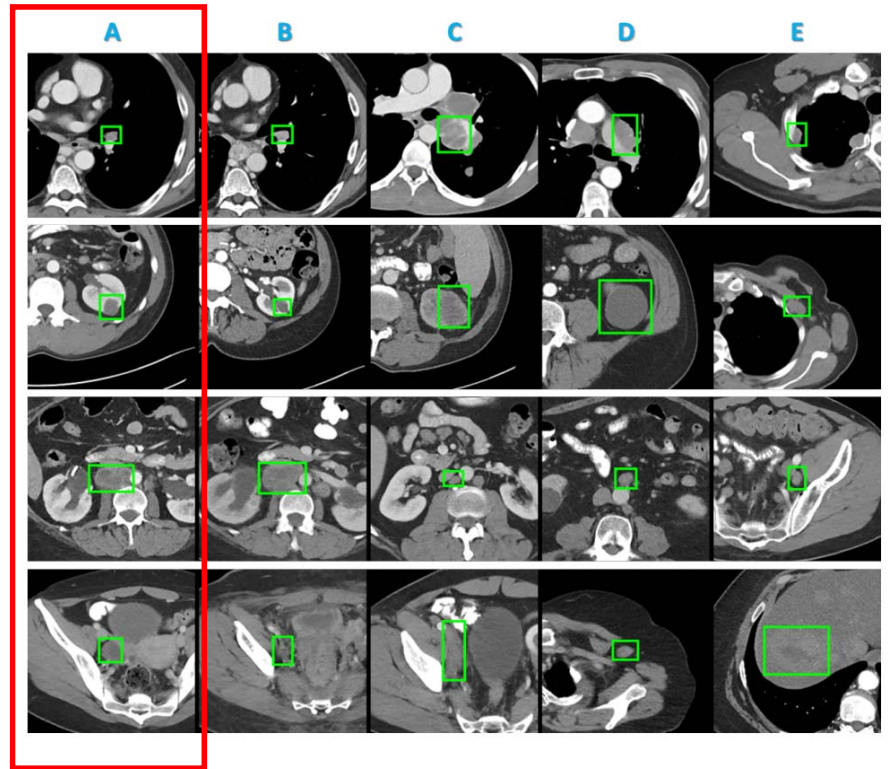


Figure 3. Sample training sequences. Each row is a sequence. Columns 1–5 are examples of lesions A–E in Fig. 1, respectively.

Triplet Network with Sequential Sampling

- Joint Loss function
 - A selected sequence of 5 instances can be decomposed into three triplets: $\{ABC, ACD \text{ and } ADE\}$; Joint Loss \rightarrow
- Iterative refinement learning
 - With the learned similarity embedding, we can retrain the lesion type classifier to get “cleaner” pseudo-labels (using **deep embedding features**), then fine-tune the triplet network with a lower learning rate

$$\begin{aligned} L = \frac{1}{2S} \sum_{i=1}^S & [\max(0, d_{AB}^2 - d_{AC}^2 + m_1) \\ & + \max(0, d_{AC}^2 - d_{AD}^2 + m_2) \\ & + \max(0, d_{AD}^2 - d_{AE}^2 + m_3)] \\ m_3 > m_2 > m_1 > 0 \end{aligned}$$

Network Architecture

- Backbone: VGG-16
- Multi-scale, multi-crop
- Output: a deep **1408D** feature embedding vector for each lesion instance (@various of image sizes/dimensions, @1 mm/pixel)

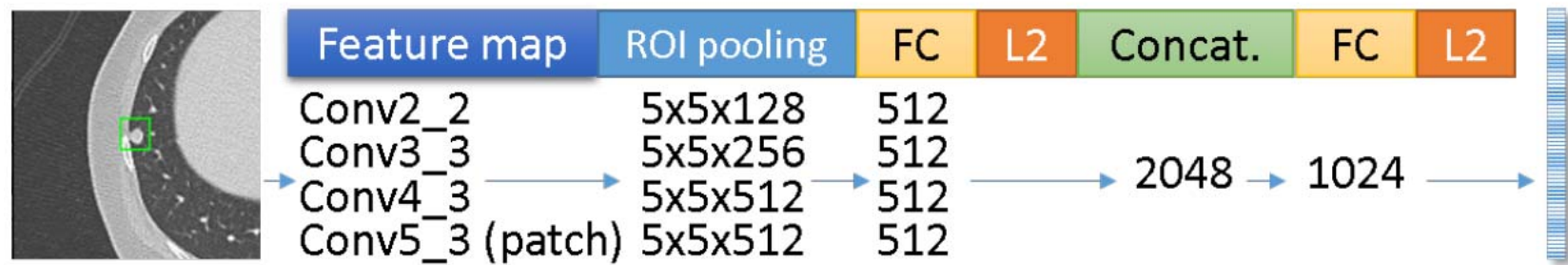


Figure 4. Network architecture of the proposed triplet network.

Lesion Organization: Retrieval & Matching

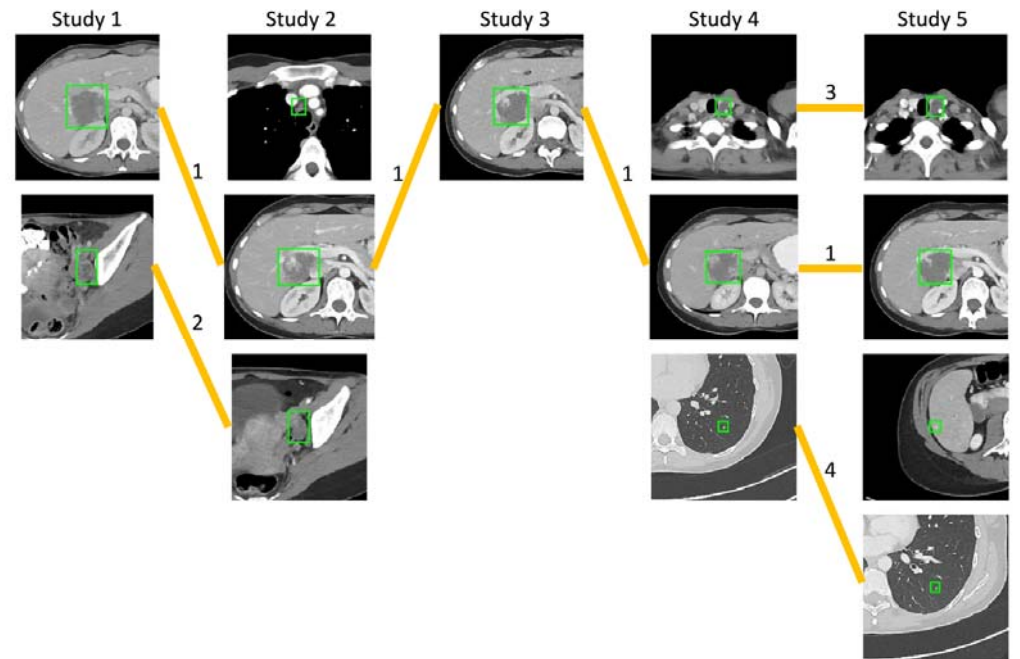
- **Inter-patient** content-based **lesion retrieval**: finding nearest neighbors of query lesions → data-learned similarity score permitting!
- **Intra-patient lesion matching:**
graph-based edge pruning

Algorithm 1 Intra-patient lesion matching

Input: Lesions of the same patient represented by their embeddings; the study index s of each lesion; intra-study threshold T_1 ; inter-study threshold T_2 .

Output: Matched lesion groups.

- 1: Compute an intra-patient lesion graph $G = \langle V, \mathcal{E} \rangle$, where V are nodes (lesions) and \mathcal{E} are edges. Denote d_{ij} as the Euclidean distance between nodes i, j .
 - 2: **Merge** nodes i and j if $s_i = s_j$ and $d_{ij} < T_1$.
 - 3: **Threshold**: $\mathcal{E} \leftarrow \mathcal{E} - \mathcal{D}, \mathcal{D} = \{\langle i, j \rangle \in \mathcal{E} | d_{ij} > T_2\}$.
 - 4: **Exclusion**: $\mathcal{E} \leftarrow \mathcal{E} - \mathcal{C}, \mathcal{C} = \{\langle i, j \rangle | \langle i, j \rangle \in \mathcal{E}, \langle i, k \rangle \in \mathcal{E}, s_j = s_k, \text{and } d_{ij} \geq d_{ik}\}$.
 - 5: **Extraction**: Each node group with edge connections is considered as a matched lesion group.
-



Implementation Details: Image Preprocessing

- Rescale image intensity to floating-point numbers in [0, 255] using a single windowing (-1024 ~ 3071 HU)
- Resize spacing to 1 mm/pixel
- Crop a patch with 50 mm padding around each lesion's bounding-box
- Use 3 neighboring slices (interpolated at 2 mm inter-slice intervals) to encode 3D information
- No data augmentation was used

Implementation Details: Training Schemes

- The maximum value of each dimension of the locations and sizes is normalized to 1

$$m_1 = 0.1, m_2 = 0.2, m_3 = 0.4$$

- 24 five-instance sequences per mini-batch
- SGD with a learning rate of 0.002, reduced to 0.0002 at iteration 2K#, converges in 3K iterations
- To train SSBR, we used 800 random unlabeled CT volumes of 420 subjects from ***DeepLesion*** patient population

Experiments

- Visualization of DeepLesion: projecting lesion **densely-connected hyper-graph** into a 2D map (*t-SNE*) !
- *X*- and *Y*-axes of the scatter map correspond to the *X*- and *Z*-coordinates of the **relative body location** of each lesion → organized by lesion type, then location!
- Illustration of the **distribution diversity** of *DeepLesion* dataset (<https://arxiv.org/abs/1710.01766>)

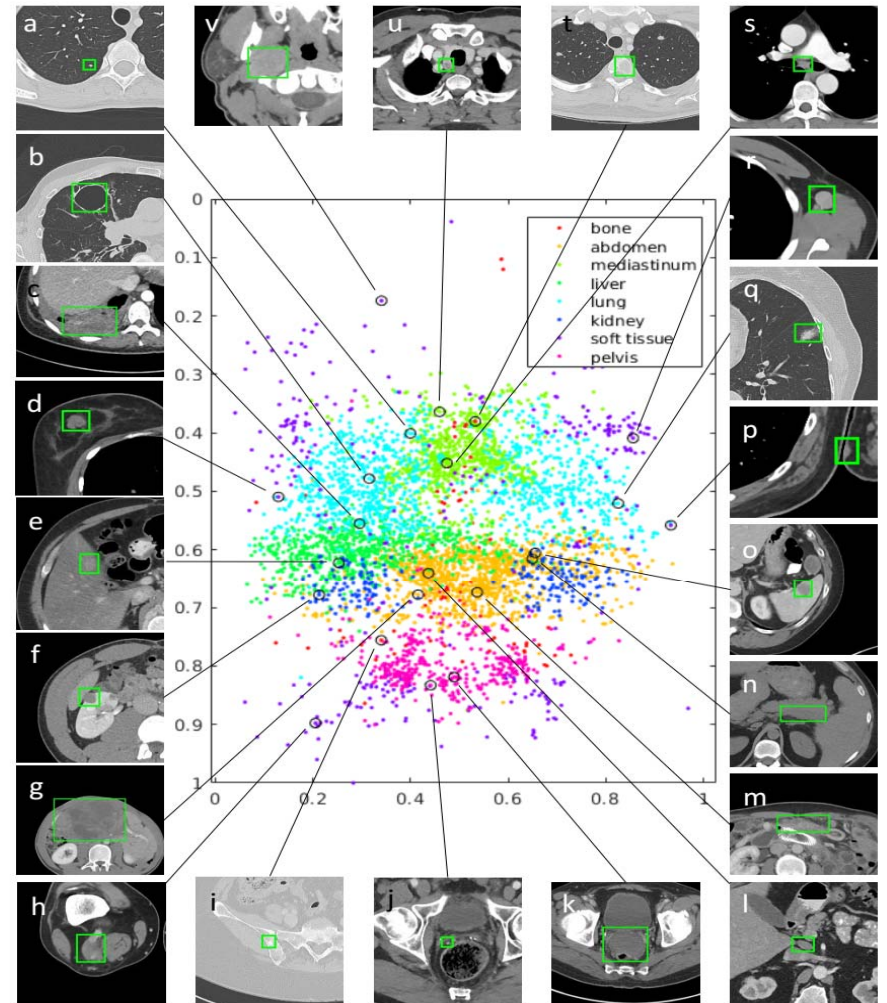


Figure 3. Visualization of the DeepLesion dataset (test set). The *x*- and *y*-axes of the scatter map correspond to the *x*- and *z*-coordinates of the relative body location of each lesion, respectively. Therefore, this map is similar to a frontal view of the human body. Colors indicate the manually labeled lesion types. Sample lesions are exhibited to show the great diversity of DeepLesion, including: a. lung nodule; b. lung cyst; c. costophrenic sulcus (lung) mass/fluid; d. breast mass; e. liver lesion; f. renal mass; g. large abdominal mass; h. posterior thigh mass; i. iliac sclerotic lesion; j. perirectal lymph node (LN); k. pelvic mass; l. periportal LN; m. omental mass; n. peripancreatic lesion; o. splenic lesion; p. subcutaneous/skin nodule; q. ground glass opacity; r. axillary LN; s. subcarinal LN; t. vertebral body metastasis; u. thyroid nodule; v. neck mass.

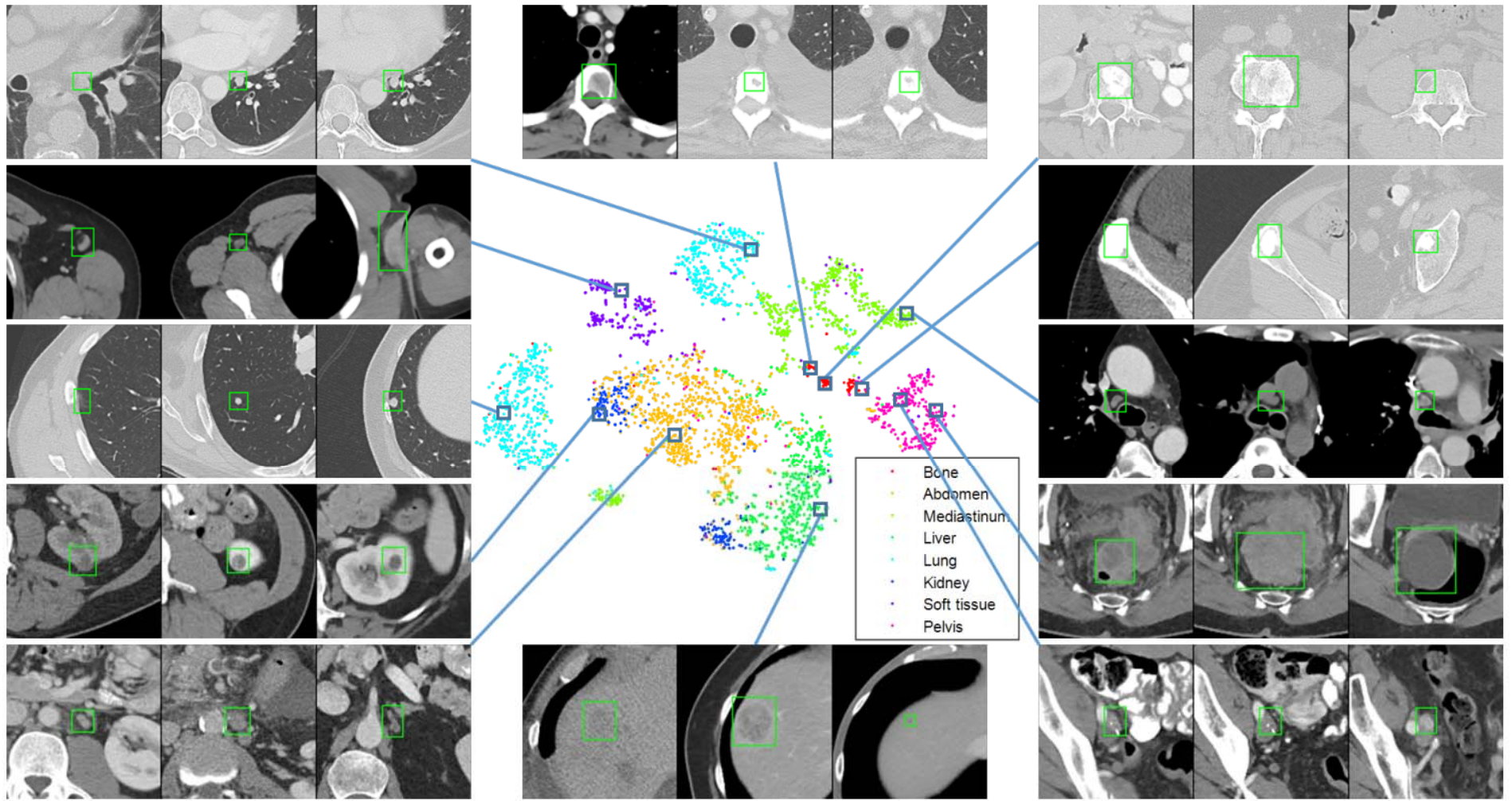


Figure 5. t-SNE visualization of the lesion embeddings on the test set (4,927 samples) of DeepLesion. Colors indicate the manually labeled lesion types. We also split the samples to 128 clusters using K-means and show 3 random lesions in 12 representative clusters. We did not choose to show closest samples because they are very similar. Best viewed in color.

Experiments: Lesion Retrieval

Multi-scale Deep Lesion Appearance Vector via Triplet Network to encode lesion type, location and size (thus sub-types)!

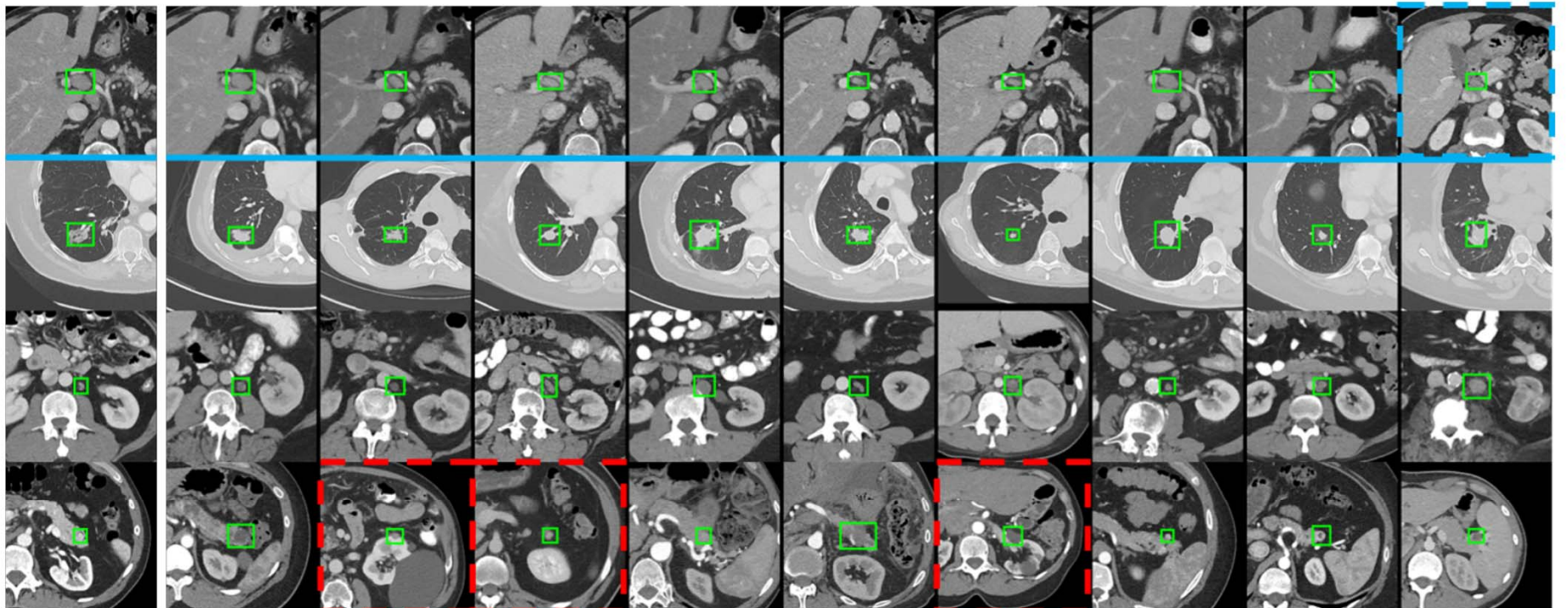


Figure 6. Examples of query lesions (first column) and the top-9 retrieved lesions on the test set of DeepLesion. In the first row, the blue dashed box marks the lesion from a different patient than the query one, whereas the other 9 are all from the same patient. In rows 2–4, we constrain that the query and all retrieved lesions must come from different patients. Red dashed boxes indicate incorrect results, see text.
10/28/2018

Longitudinal Intra-patient Lesion Matching

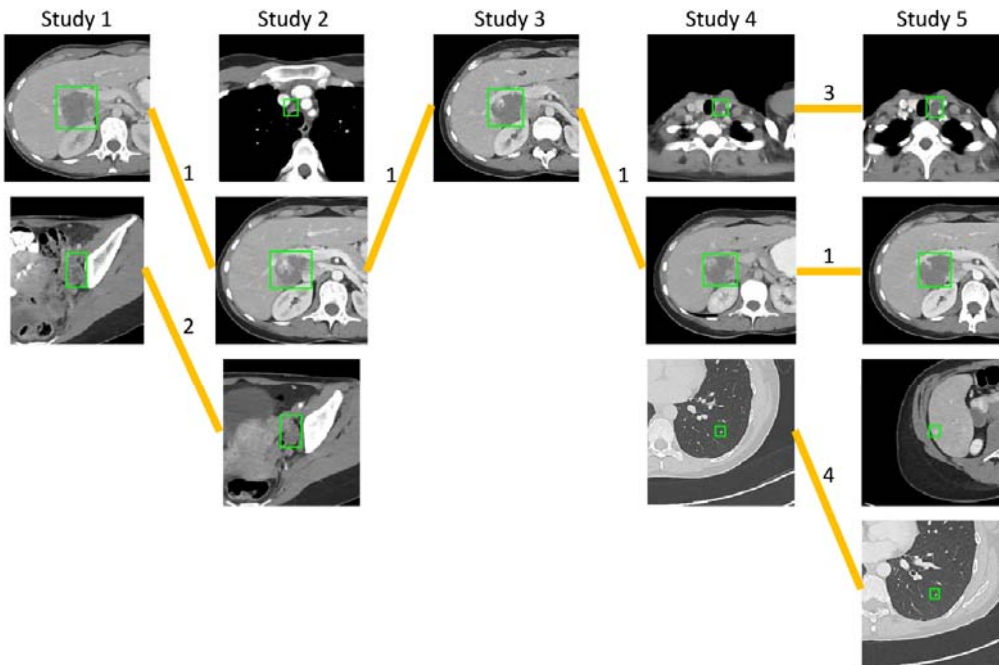


Figure 5. All lesions of a sample patient in DeepLesion. Lesions in each study (CT examination) are listed in a column. Not all lesions occur in each study, because the scan ranges of each study vary and radiologists only mark a few target lesions. We group the same lesion instances to sequences. Four sequences are found and marked in the figure, where the numbers on the connections represent the lesion IDs.

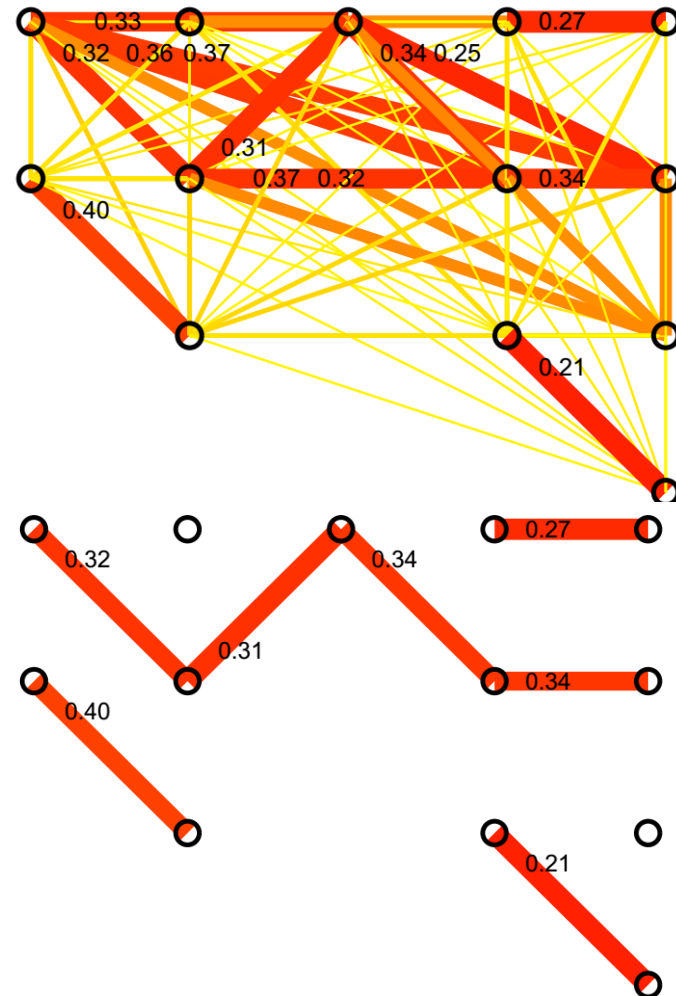
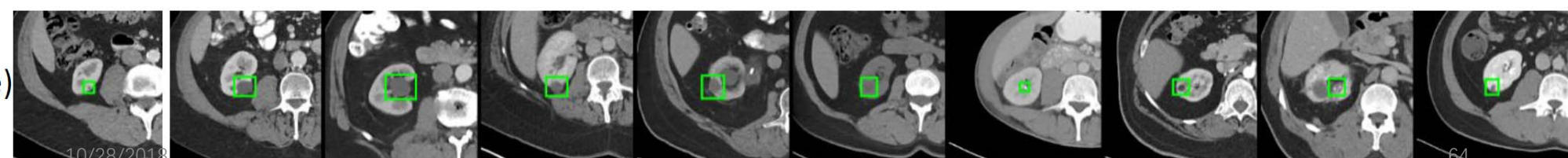
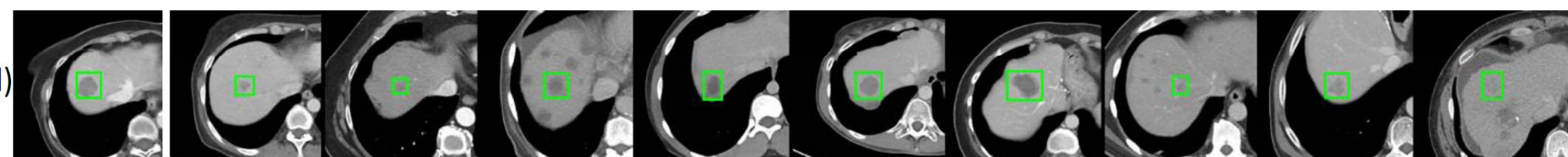
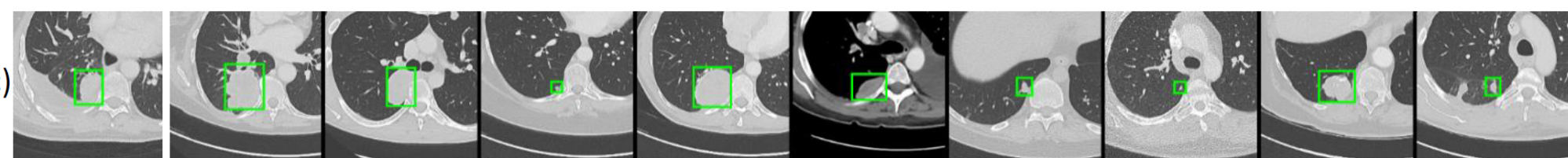
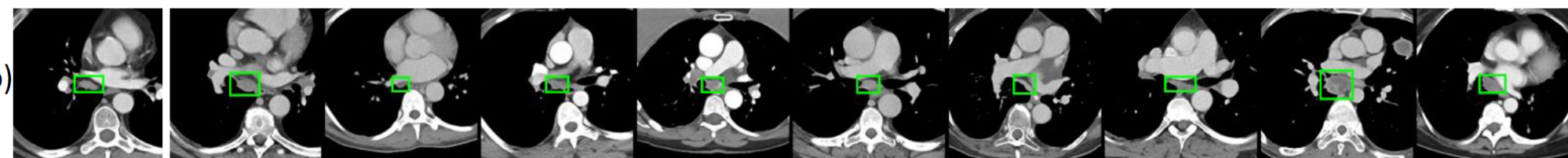
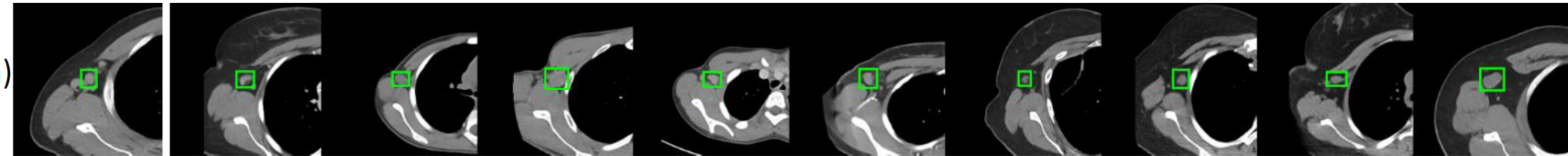


Figure 7. The final lesion sequences found by processing the lesion graph in Fig. 6 using Algo. 1 in the paper. They are the same with the ground-truth in Fig. 5.



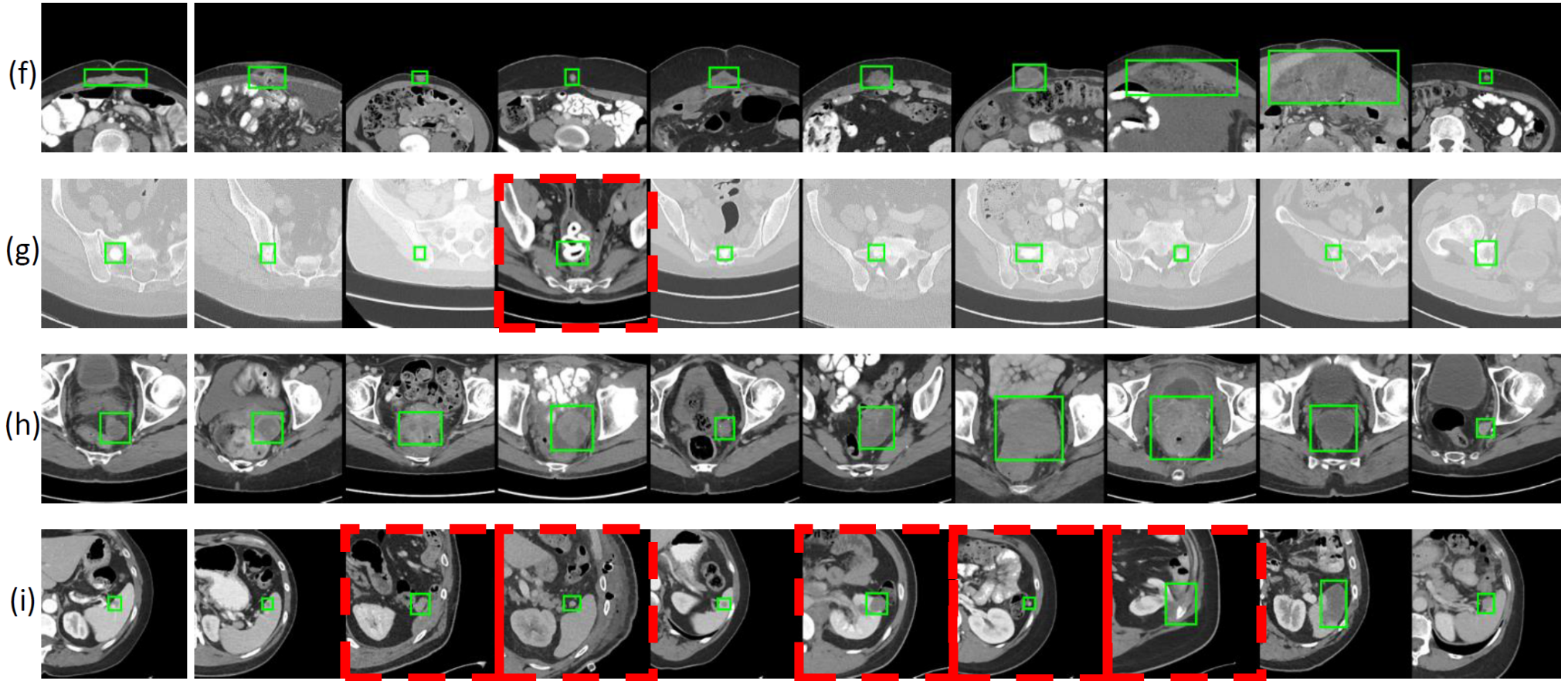


Figure 4. More examples of query lesions (first column) and the top-9 retrieved lesions on the test set of DeepLesion. We constrain that the query and all retrieved lesions must come from different patients. Red dashed boxes indicate incorrect results. The lesions in each row are: (a) Right axillary lymph nodes; (b) subcarinal lymph nodes; (c) lung masses or nodules near the pleura; (d) liver lesions near the liver dome; (e) right kidney lesions; (f) lesions near the anterior abdomen wall; (g) lesions on pelvic bones except the one in the red box, which is a peripherally calcified mass. (h) inferior pelvic lesions; (i) spleen lesions except the ones in red boxes.

Summary

- We present a large-scale and comprehensive dataset, **DeepLesion**, including significant radiology image findings mined from PACS
 - can be used for multi-category lesion detection, retrieval, classification, segmentation, …, **the first study of its kind!**
- **Lesion Graph Embedding** is learned with a triplet network to model their similarity relationship in type, location, and size
 - The only manual efforts needed are the class labels of some seed images
 - **Non-parametric deep** radiology instance/knowledge representation
- Promising results are obtained in (a) inter-patient **content-based lesion retrieval** and (b) intra-patient **lesion matching**, qualitatively and quantitatively.

[5] Liu, Lu, Ye, Yu, Huang: Coarse-to-fine classification via parametric and **nonparametric models for computer-aided diagnosis**. ACM CIKM 2011

Acknowledgement

- **Scientific Collaborators:** Holger Roth, Hoochang Shin, Xiaosong Wang, Ke Yan, Ling Zhang, Adam P. Harrison, Jinzheng Cai, Youbao Tang, Yuxing Tang, Jianhua Yao, Ari Seff, Isabella Nogues, Mingchen Gao, Yifan Peng, Jiamin Liu, Amal Farag, Ziyue Xu, Zhiyong Lu, Jing Xiao, Lin Yang, Nathan Lay
- **Clinical Collaborators:** Lauren Kim (MD), Mohammadhad Bagheri (MD), Ronald M. Summers (MD/PhD), Evrim Turkbey (MD)
- **Funding:** NIH Clinical Center Intramural Research Program, NIH-PingAn CRADA, NVIDIA GPU grants

What's next?

"Clinician Lead Technology powered novel & effective clinical workflows that translate"

<https://www.nih.gov/about-nih/what-we-do/nih-almanac/lasker-awards>

Improve patient care through Harmonization of computing intelligence and clinical sciences/practices